Gaseous Tracking Detectors at e^+e^- colliders

F. Grancagnolo

Летняя научная школа "Супер с-тау фабрика"

25-29 July 2022

НЦФМ, МГУ (Саров)

Tracker alternatives for future colliders

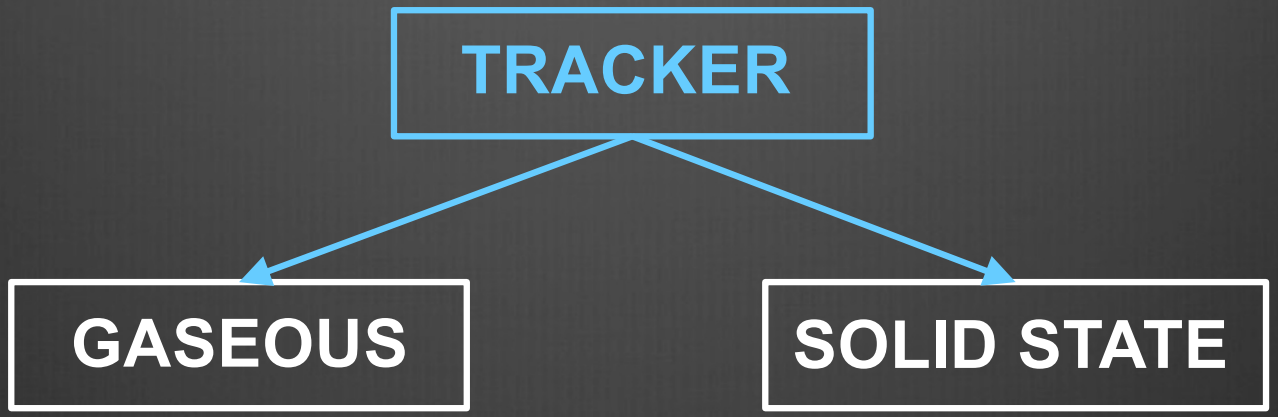

Solid state tracker drawbacks

- **multiple scattering**
  - contribution to momentum resolution due to multiple scattering larger than in a gaseous tracker and dominant up to large momenta
- **redundancy**
  - only a limited number N of layers can be implemented: momentum resolution proportional to σ/√N, the excellent spatial resolution σ can be compensated by N (25 μm/√6 ≈ 100 μm/√100)
  - inefficiencies in the reconstruction of "kinks" and "vees"
  - lack of redundancy against hit inefficiencies and background hits
- **particle identification**
  - no effective particle identification possible (maybe TOF)
- **system complexity**
  - order of 10^9 readout channels for a limited number of space points on tracks with lever arms compatible with the momenta to be measured
  - complex alignment systems and their relative and absolute stabilities

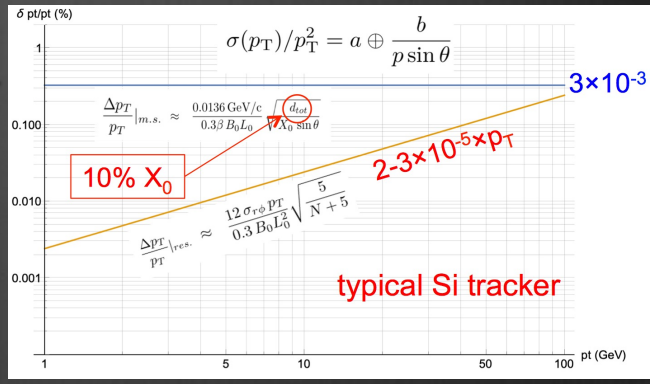

Drasal and Riegler, https://doi.org/10.1016/j.nima.2018.08.078

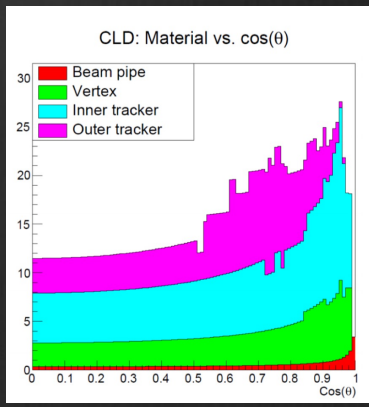

Tracker alternatives for future colliders

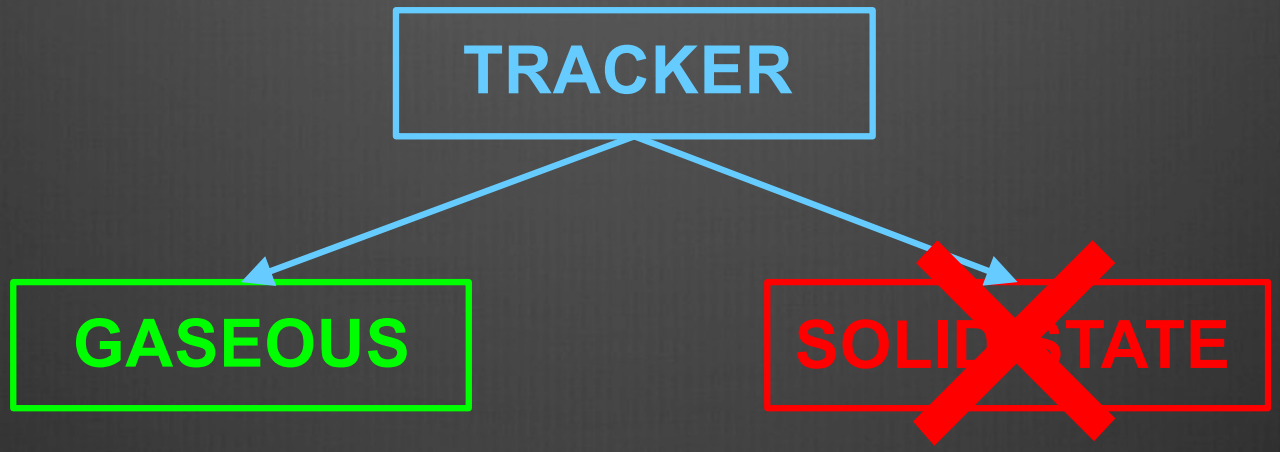

Tracker alternatives for future colliders

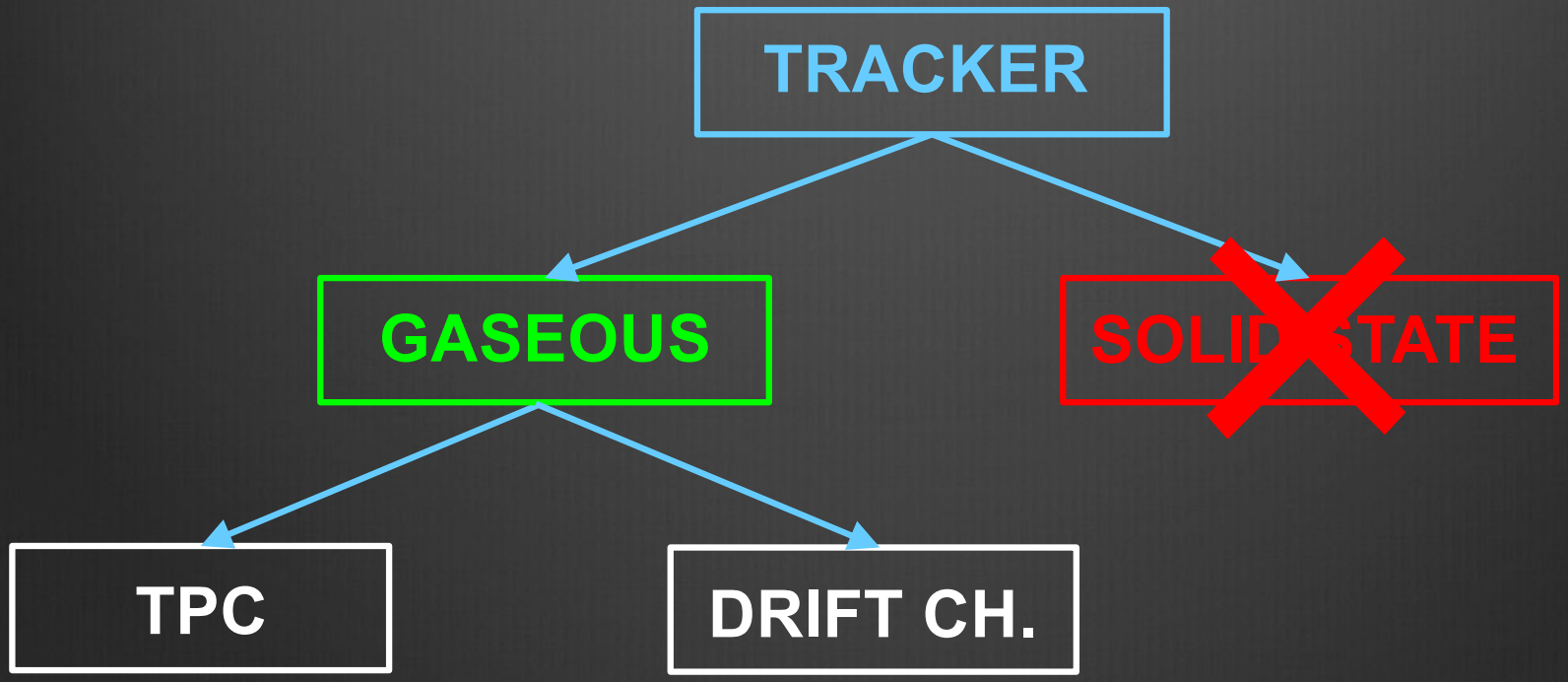

A due tribute …

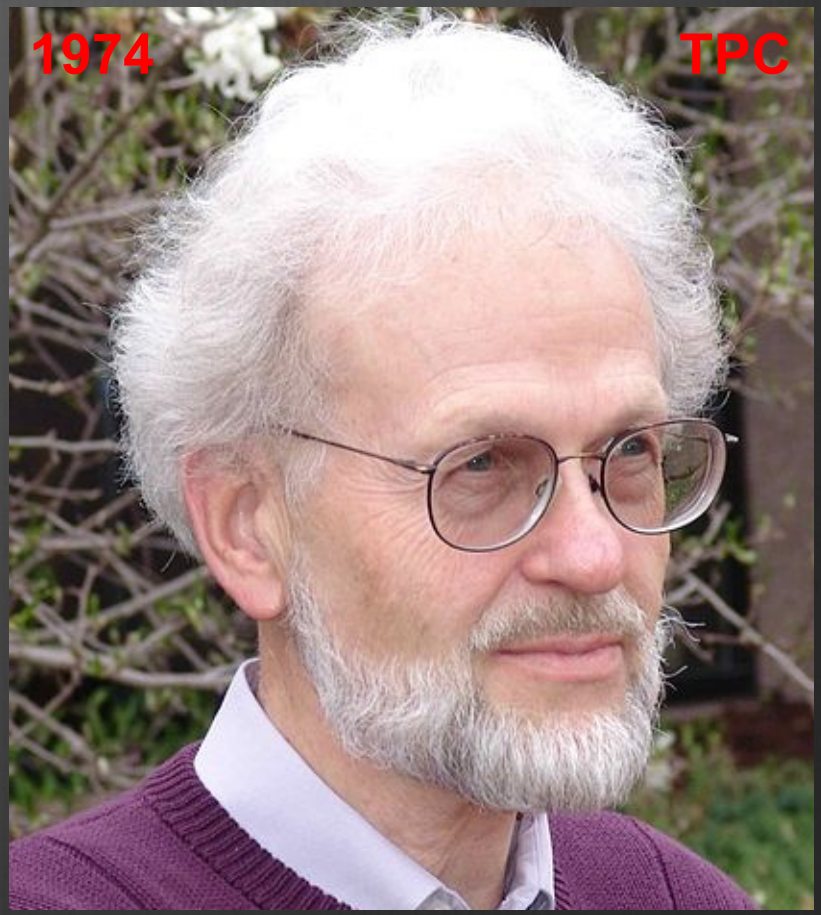

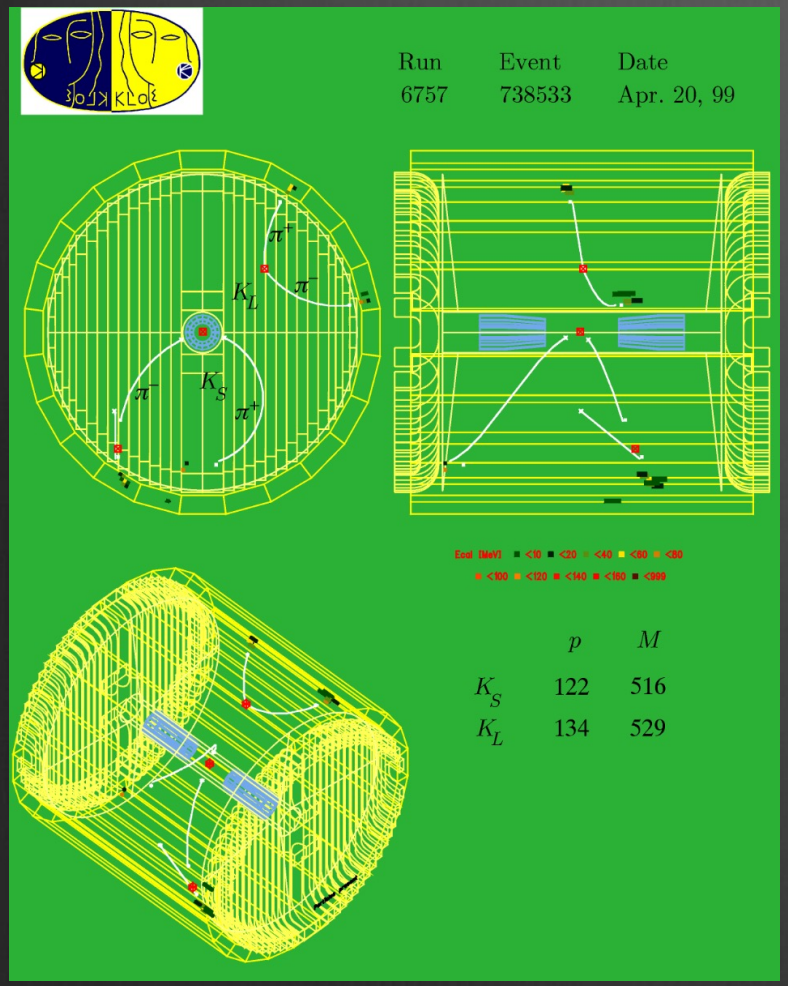
Run Event Date
6757 738533 Apr. 20, 99
π^+
K_L
π^-
K_S
π^-
π^+
Eccl [MeV] <10 <20 <40 <60 <80
<100 <120 <140 <160 <999
p M
K_S 122 516
K_L 134 529

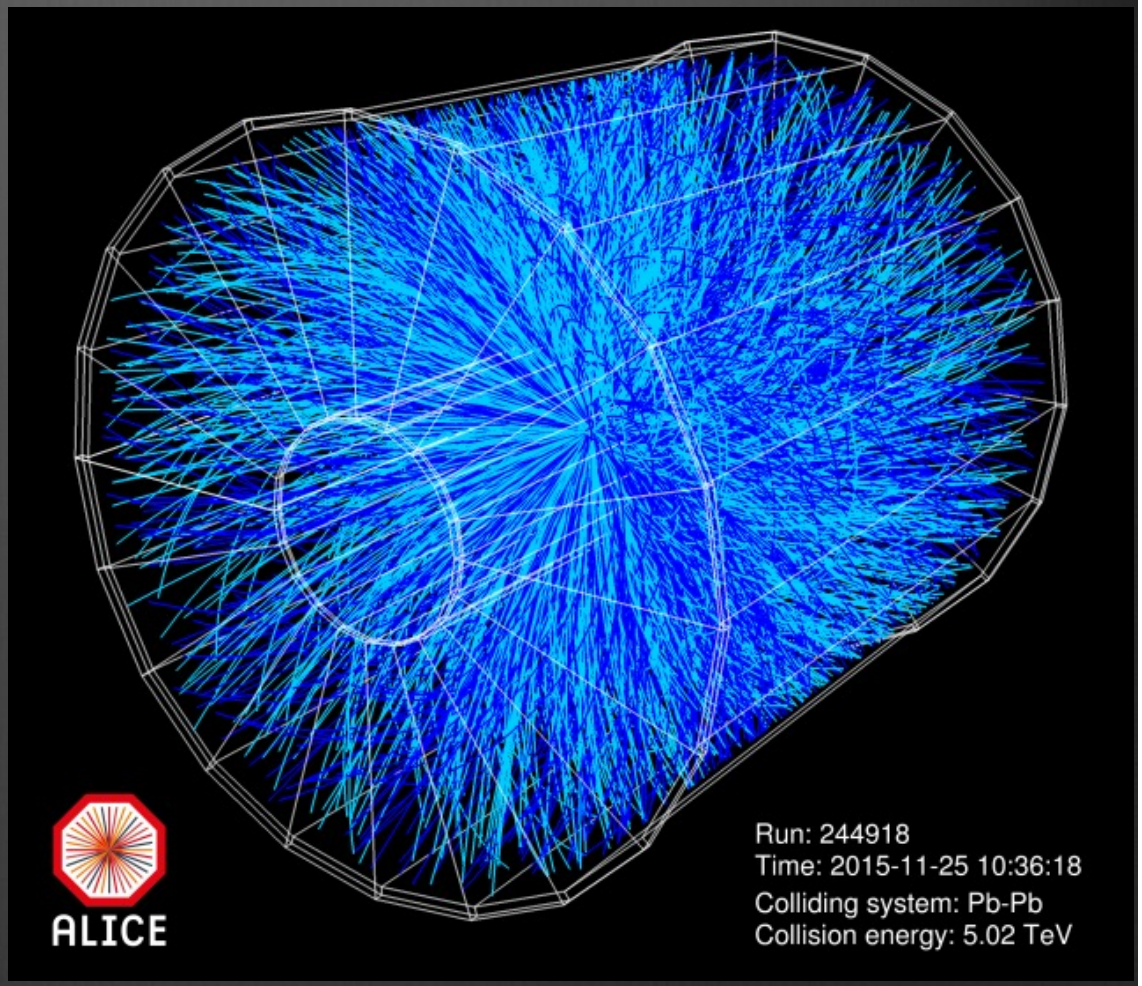
ALICE
Run: 244918
Time: 2015-11-25 10:36:18
Colliding system: Pb-Pb
Collision energy: 5.02 TeV

TPC drawbacks

- **very long drift time**
  - integrating over many bunch crossings
  - tracking resolution limited by transverse diffusion and, therefore, by B-field
- **positive ions backflow**
  - difficult implementation of efficient gating strategies (due to very short bunch lengths)
  - ion space charge density affects ion backflow, particularly at smaller radii, complicating the matching of inner track segments with vertex detector tracks in high multiplicity events and in dense particle jets
- **number of readout channels**
  - the required spatial resolution claims for readout pad sizes of a few mm^2 for a total of the order of million channels per endplate
  - consequently, sophisticated cooling systems are required
- **multiple scattering**
  - expected > 25% of a radiation length in the endplate regions and a not negligible amount in the inner wall due to the field cage structure

Tracker alternatives for CEPC

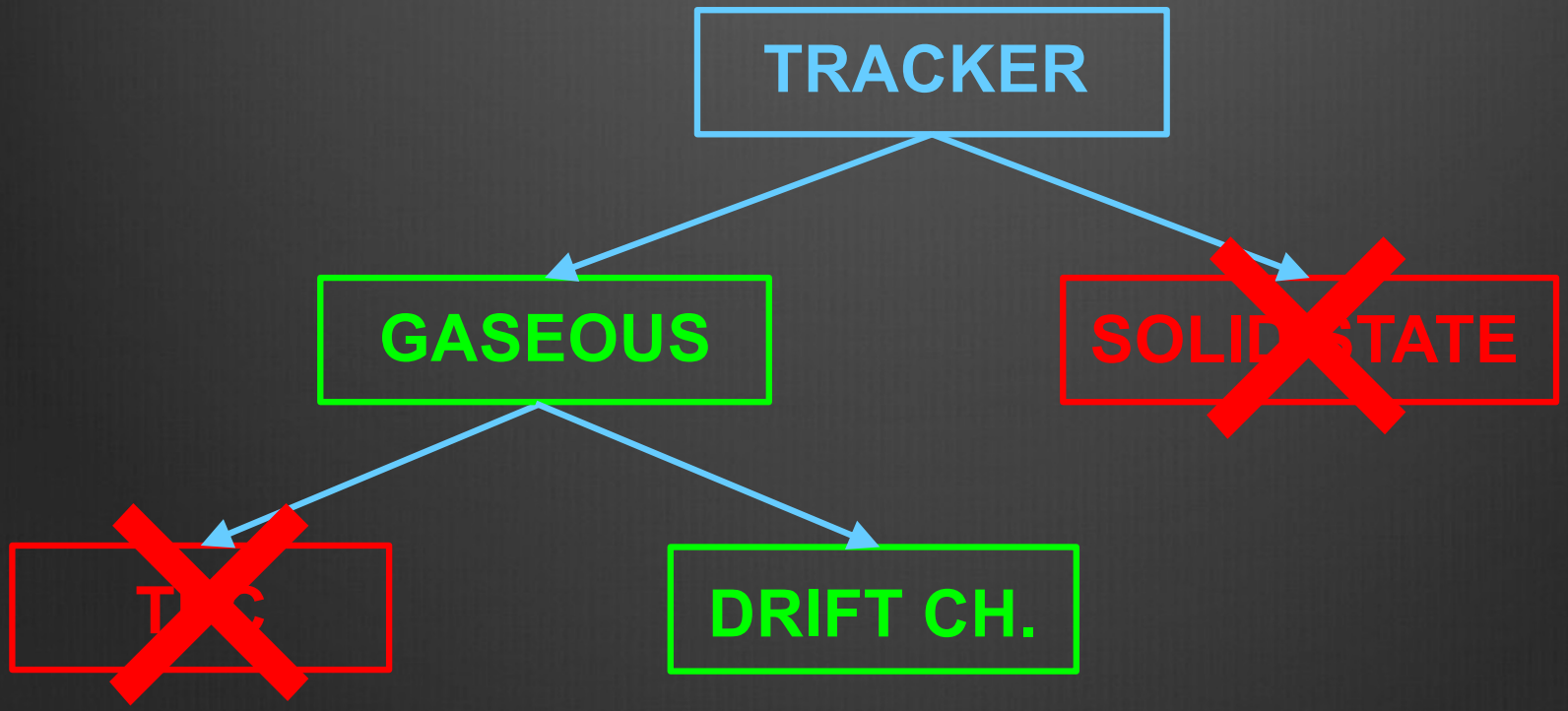

The evolution of Drift Chambers at e^+e^- colliders

- **Performance evolution**
  - Momentum Resolution
  - dE/dx, dN/dx and PId
  - Mechanical Structure (X_0)
  - FE and RO Electronics → not discussed here

- **Only Cylindrical Drift Chambers**
  - No **Planar** Drift Chambers
  - No **Time Projection** Chambers
  - No **Time Expansion** Chambers
  - No **Radial** Drift Chambers:
    radial wires − H1-forward/HERA
    radial drift − ASTERIX/CERN
  - No **Straw Tube** Cyl. Chambers (GlueX, PANDA)
- **Only e^+e^- colliders**
  - No **fixed target** configurations (MEG2)
  - No **ep and pp colliders** (AFS, CDF-CTC/COT)

- **Layout Evolution**
  - From **single** sense wire cell, to **multiple** sense wires and **jet** cell configurations - and back to **single** sense wire cell
  - **Axial-stereo** and **full stereo** layer configuration (KLOE, 4th-Concept, MEG2, IDEA)
- **Gas mixture Evolution**
  - From **Argon** to **Helium** based gas
- **Mechanical Structure and Wires Evolution**
- **Read-out: from first clusters timing to Cluster Counting and Cluster Timing**

Trackers at e^+e^- Colliders

past

SPEAR	MARK2	Drift Chamber
	MARK3	Drift Chamber
DORIS	PLUTO	MWPC
	ARGUS	Drift Chamber
CESR	CLEO1,2,3	Drift Chamber
VEPP2/4M	CMD-2	Drift Chamber
	KEDR	Drift Chamber
	NSD	Drift Chamber
PETRA	CELLO	MWPC + Drift Ch.
	JADE	Drift Chamber
	PLUTO	MWPC
	MARK-J	TEC + Drift Ch.
	TASSO	MWPC + Drift Ch.
TRISTAN	AMY	Drift Chamber
	VENUS	Drift Chamber
	TOPAZ	TPC

PEP	MARK2	Drift Chamber
	PEP-4	TPC
	MAC	Drift Chamber
	HRS	Drift Chamber
	DELCO	MWPC
BEPC	BES1,2	Drift Chamber
LEP	ALEPH	TPC
	DELPHI	TPC
	L3	Si + TEC
	OPAL	Drift Chamber
SLC	MARK2	Drift Chamber
	SLD	Drift Chamber
DAPHNE	KLOE	Drift Chamber
PEP2	BaBar	Drift Chamber
KEKB	Belle	Drift Chamber

present

VEPP2000	CMD-3	Drift Chamber
VEPP4	KEDR	Drift Chamber
BEPC2	BES3	Drift Chamber
S.KEKB	Belle2	Drift Chamber

future

ILC	ILD	TPC	
	SiD	Si	
CLIC	CLIC	Si	
FCC-ee	CLD	Si	
	IDEA	Drift Chamber	
CEPC	Baseline	TPC	Si
	IDEA	Drift Chamber	
SCTF	Sarov	Drift Chamber	
STCF	HIEPA	Drift Chamber	

MARK II at SPEAR (1978)

where it all began ...

Davies-White, W.A. *et al , A Large Cylindrical Drift Chamber for the Mark II Detector at SPEAR,* NIM 160 (1979) 227

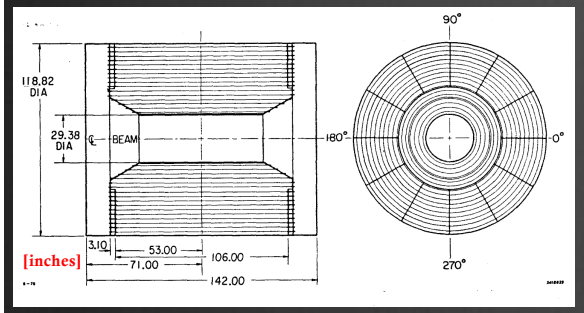

Single sense wire cell

≈ 3 m diameter

≈ 2.7 m active length

0.41 Tesla B-field

16 layers

6 axial + 10 stereo (±3°)

3204 drift cells (3:1)

22,000 wires

50% Ar – 50% C_2H_6

2% X_0 radial - 20% X_0 e.p.

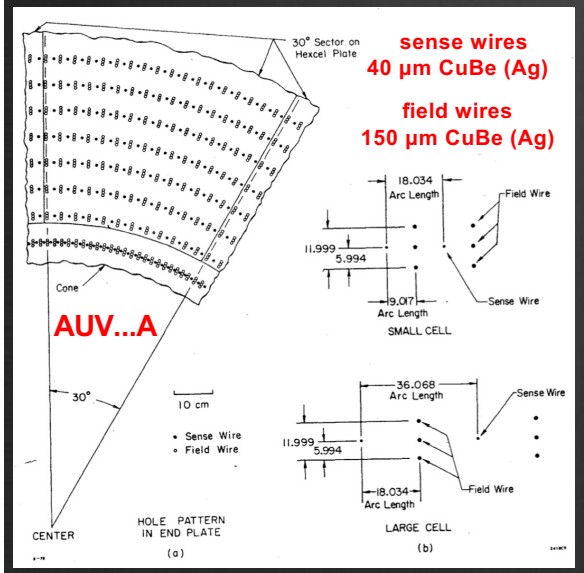

sense wires
40 μm CuBe (Ag)

field wires
150 μm CuBe (Ag)

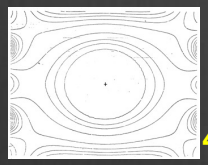

equi-time contours

max drift time
450 ns (780 ns BX)

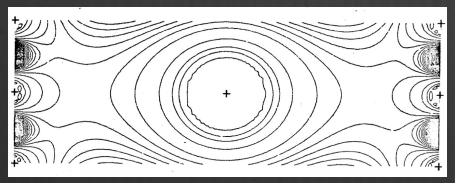

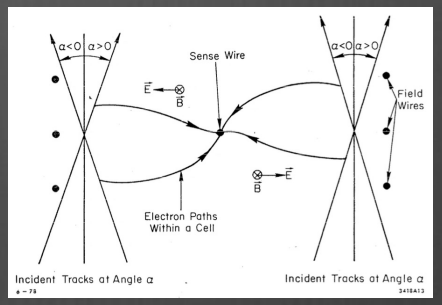

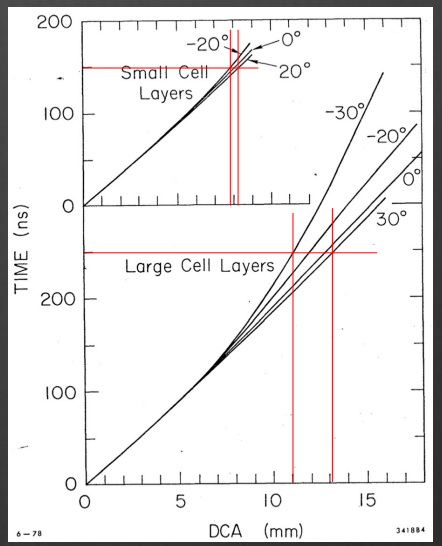

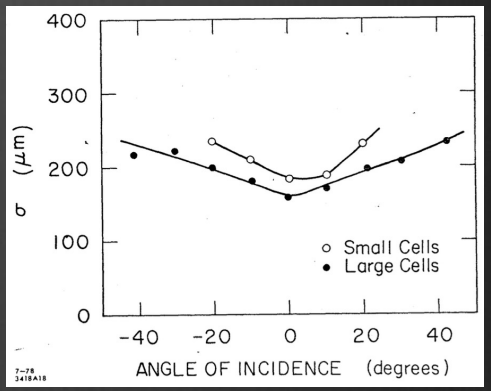

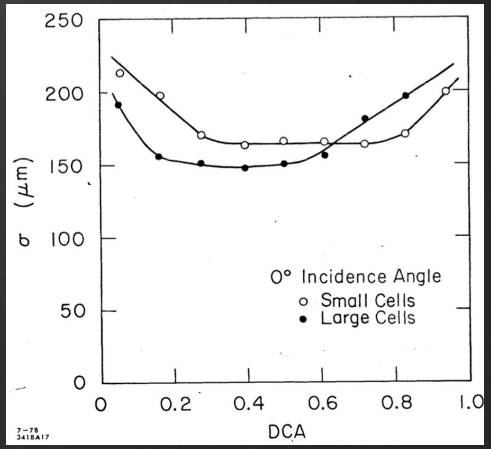

Single sense wire "open" cells 3:1

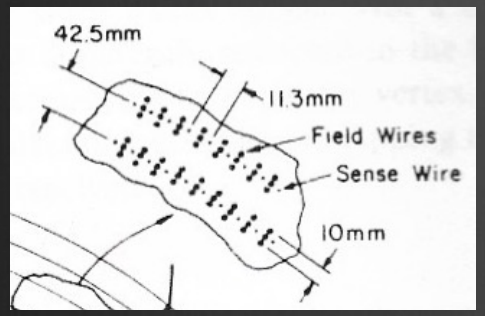

CLEO
CESR
1979

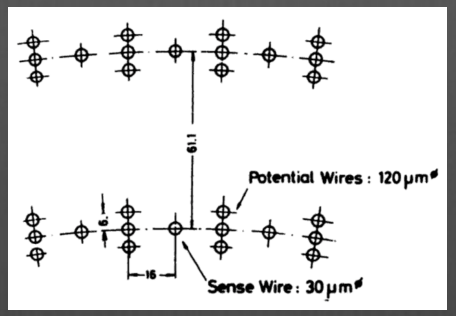

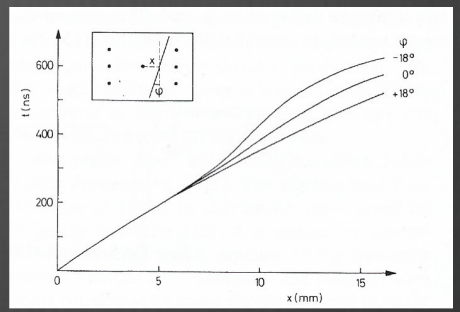

TASSO
PETRA
1979

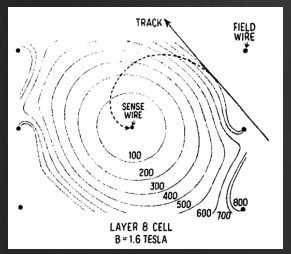

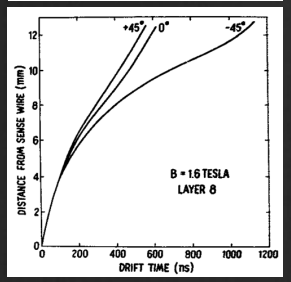

HRS
PEP
1980

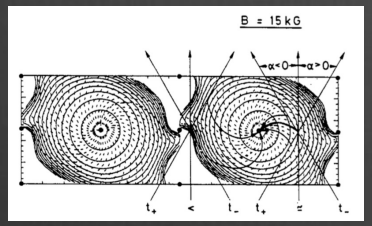

CELLO
PETRA
1980

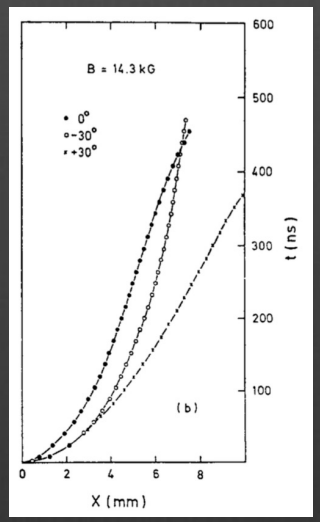

VENUS
TRISTAN
1983

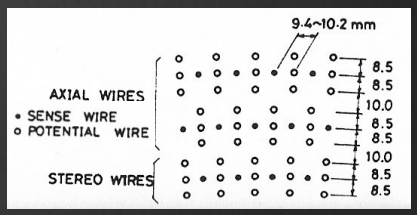

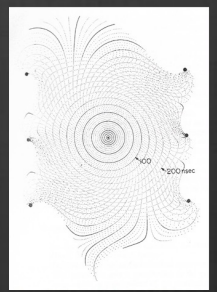

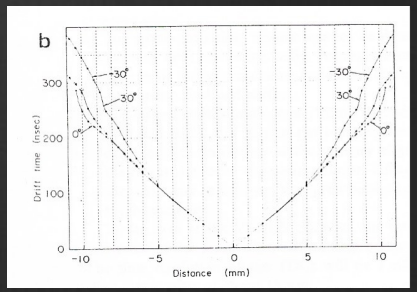

Single sense wire "open" cells 3:1 Layout

	MARK II SPEAR (1978)	CLEO CESR (1979)	TASSO PETRA (1980)	CELLO PETRA (1980)	HRS PEP (1980)	VENUS TRISTAN (1985)
Inner Radius [mm]	370	172	320	170	152	250
Outer Radius [mm]	1450	950	1280	700	1100	1260
Length [mm]	2700	1930	3450	2200	2540	3000
Axial layers	6	9	9	7	7	20
Stereo layers	10	8	6	0	8	9
Stereo angles [mrad]	±52	±52	±70	0	±60	±60
Number of sense wires	3204	5304	2340	1312	2448	7104
Total number of wires	13,000	22,000	9,000	5,200	10,000	28,000
sense wires [μm]	40 Cu-Be(Ag)	20 W(Au)	30 W(Au)	20 W(Au)	37 W(Au)	30 W-Re(Au)
field wires [μm]	150 Cu-Be(Ag)	115 Cu-Be(Ag)	120 Mo(Au)	50-100 Cu-Be	127 Cu-Be(Au)	125 Cu-Be(Au)
Inner cylinder [mm/X_0]	3.2 Lexan / 0.9%		5 fiberglass/ 3%		1 Be / 0.3%	1 C-f / 0.5%
Outer cylinder [mm/X_0]	6.25 Al / 7%		6.0 Al / 7%		0.6 Al / 0.7%	5 C-f / 2.4%
End-plates [mm/X_0]	6.35 Al (cone) 3.2 Al + ... / 20%		35 Al /39%		9.5 Al (cone) 15.9 Al / 18%	21 Al / 24%

Single sense wire "open" cells 3:1 Performance

	MARK II SPEAR (1978)	CLEO CESR (1979)	TASSO PETRA (1980)	CELLO PETRA (1980)	HRS PEP (1980)	VENUS TRISTAN (1985)
B-field [T]	0.4	1.0	0.5	1.3	1.6	0.75
Cell Size [mm²]	(9÷18)×12	11.3×10	16×12	15×18	17×10 ÷ 25×12	19×17
Gas Mixture	50 Ar / 50 C_2H_6	50 Ar / 50 C_2H_6	90 Ar / 10 CH_4	90 Ar / 10 CH_4	89 Ar / 10 CO_2 / 1 CH_4	50 Ar / 50 C_2H_6
Spatial Resolution [μm]	150-200	250	220	170	200	150
Momentum Resolution	0.010p / 0.0145	0.012p / 0.007	0.020p / ?	0.029p / ?	0.005p / 0.003	0.0088p / 0.0012
Δp [MeV/c] at 1 GeV/c	17.6	13.9	>20.0	>30.0	5.8	14.9
dE/dx	//	6.5%	//	//	TOF + Cer.	//

From "open" to "closed" cells

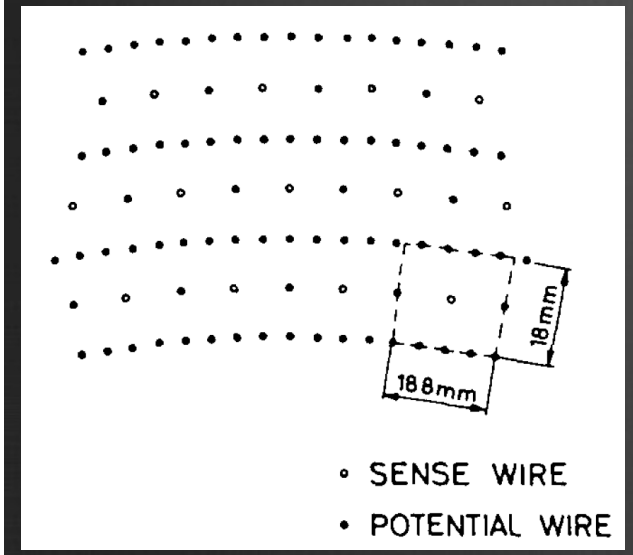

6:1
ARGUS
DORIS
1982

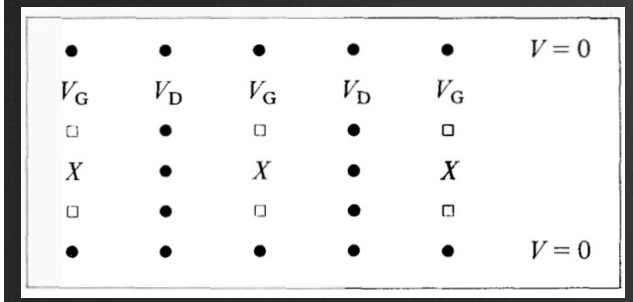

5(7):1
DM2
DCI
1982

A square-shape, closed cell implies more uniform and t-to-d relations less dependent from the track angle

A larger ratio of field to sense wires allows for thinner field wires and, therefore, for less multiple scattering contribution from the wires to the momentum measurement.

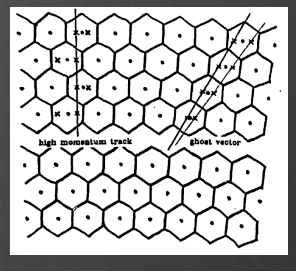

2:1
AMY
TRISTAN
1984

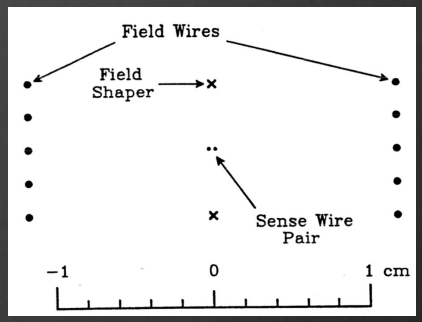

5:1
MAC
PEP
1980

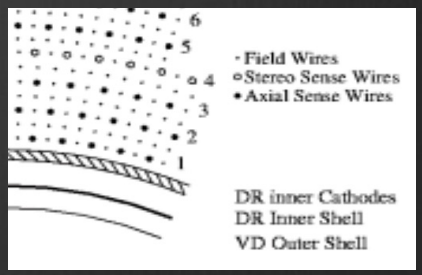

3:1
CLEO2
CESR
1985

Single sense wire "closed" cells Layout

	MAC PEP (1980)	ARGUS DORIS (1982)	DM2 DCI (1982)	AMY TRISTAN (1984)	CLEO2 CESR (1984)
Inner Radius [mm]	120	150	325	148	175
Outer Radius [mm]	455	860	871	655	945
Length [mm]	1890	2000	2400	1800	1890
Axial layers	4	18	5	25	40
Stereo layers	6	18	8	15	11
Stereo angles [mrad]	±50	±40÷80	±52	±79	±52
Number of sense wires	883	5940	2080	9048	12240
Total number of wires	6,500	31,000	17,000	32,000	49,000
sense wires [μm]	20 W(Au)	20 W-Re(Au)	20 W-Re(Au)	20 W(Au)	20 W(Au)
field wires [μm]	200 Cu-Be	120-200 Al(Au)	120-200 Al(Au)	160 Al(Au)	110 Al/Cu-Be(Au)
Inner cylinder [mm/X_0]	? / 1.6%	3.3 C-f / 1.5%			0.75 C-f+1 Al / 1.5%
Outer cylinder [mm/X_0]		6 Al / 6.7%			6.35 HC+1.6 Al/ 3%
End-plates [mm/X_0]	19 SS / 110%	30 Al / 34%			31.7 Al / 36%

Single sense wire "closed" cells Performance

	MAC PEP (1980)	ARGUS DORIS (1982)	DM2 DCI (1982)	AMY TRISTAN (1984)	CLEO2 CESR (1984)
B-field [T]	0.57	0.8	0.5	3.0	1.5
Cell Size [mm²]	(15÷23.5)×10	18×18.8	24x40	10×12	14×14
Gas Mixture	90 Ar / 10 CH_4	97 C_3H_6 / 3 $C_3H_6O_2$	50 Ar / 50 C_2H_6	50 Ne / 50 C_2H_6	50 Ar / 50 C_2H_6
Spatial Resolution [μm]	180	150	180	200	180
Momentum Resolution	0.052p / ?	0.009p / 0.010	0.014p / 0.014	0.0070p / ?	0.0026p / 0.0057
Δp [MeV/c] at 1 GeV/c	>52	13.5	19.8	>10	6.3
dE/dx	//	5.0%	TOF + Cer.	//	6.0%

Lesson #1 - from "open" to "closed" cell

- closed cells limit the very long tails in the drift time distribution
- closed cells make the time-to-distance relations less dependent from the track angle
- square cells make the time-to-distance relations more isotropic
- small drift distance limits drift asymmetries due to Lorenz angle

... but

- portions of active volume not sampled between the cylindrical envelope of axial wires and the hyperboloid envelope of stereo wires
- small ratio of the number of field wires per sense wire (3:1) forces the use of thick field wires with consequences on multiple scattering contribution to momentum resolution and total load on end-plates
- some problems with left-right ambiguity and close tracks separation

MARK3 at SPEAR – JADE at PETRA

F. Grancagnolo and A. Seiden, Large Drift Chambers with a Multi-Wire Cell Design, SCIPP 81/5

J. Heintze, Drift chambers and recent developments, NIM 156 (1978) 227

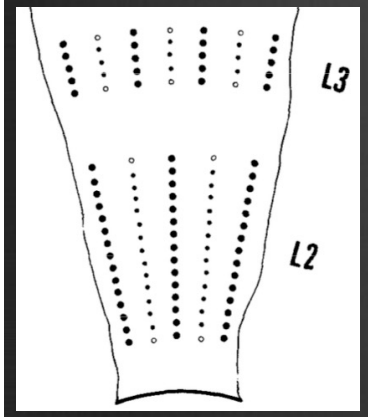

2.33:1
MARK3
SPEAR
1980

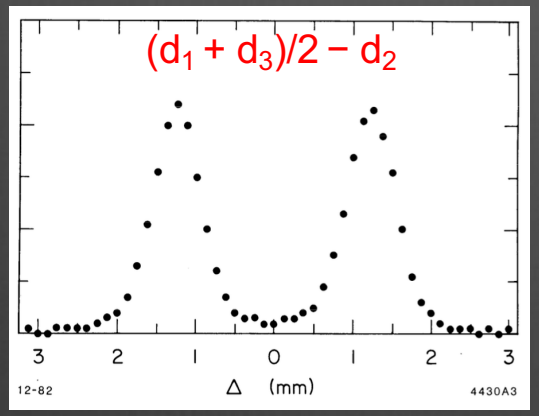

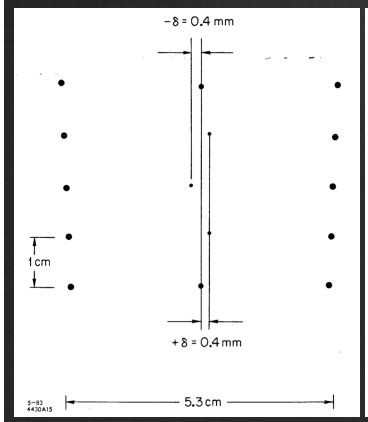

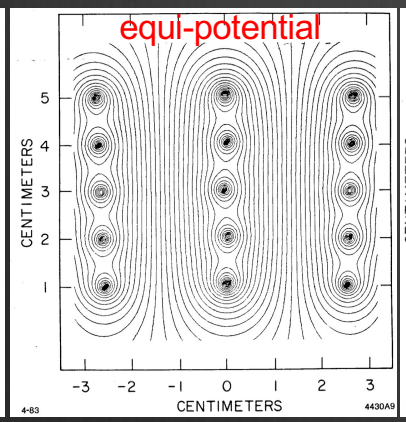

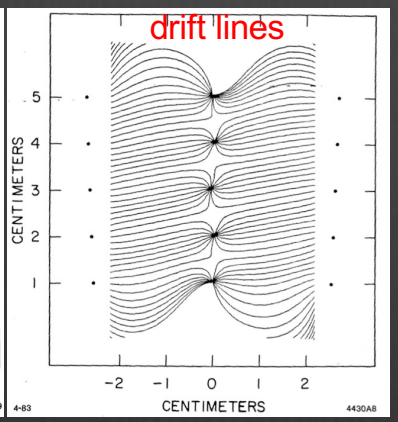

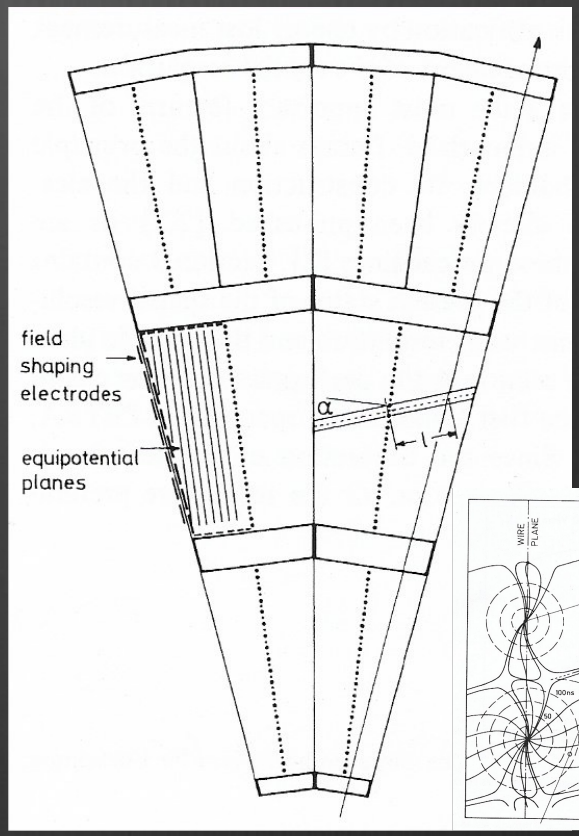

≈1:1
JADE
PETRA
1981

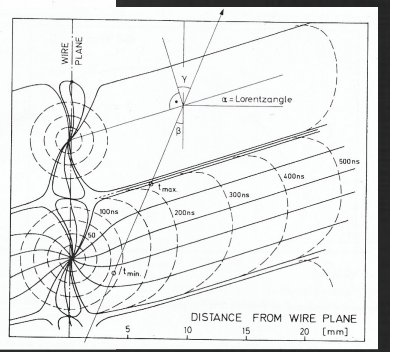

Multi-wire and Jet-like cells

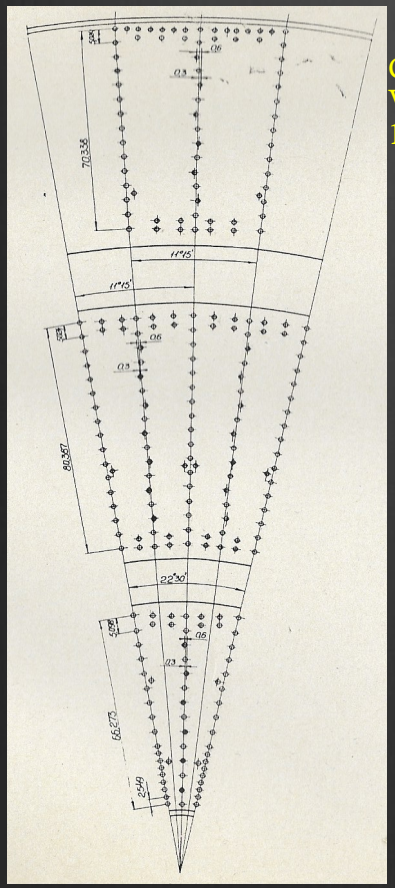

6.8:1
CMD-2
VEPP -2M
1985

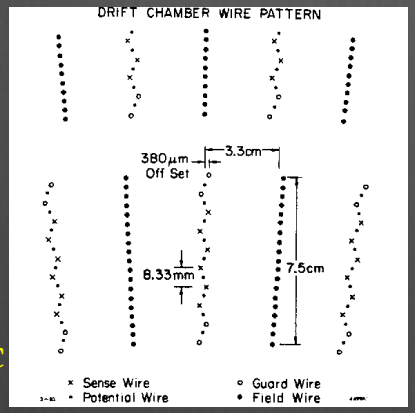

5.3:1
MARK2
PEP/SLC
1985

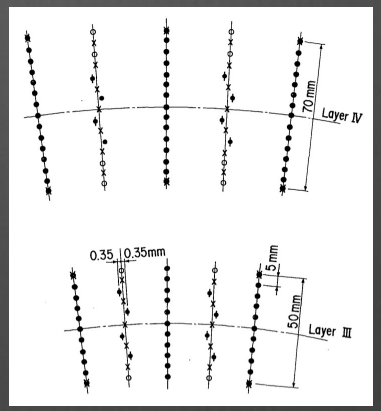

6.5:1
BES
BEPC
1989

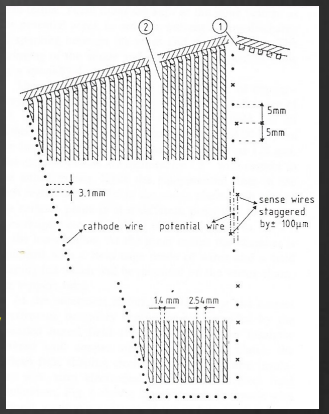

4.3:1
OPAL
LEP
1988

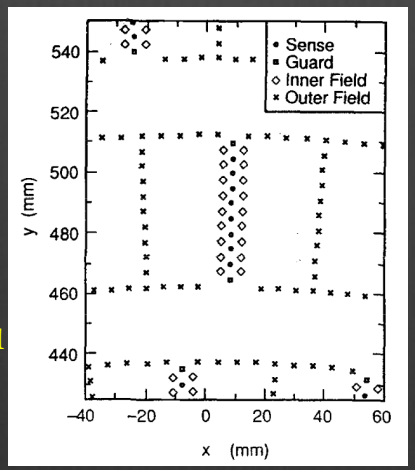

5.625:1
SLD
SLC
1988

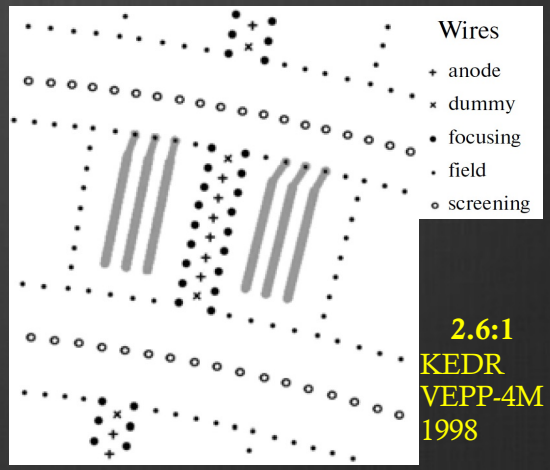

2.6:1
KEDR
VEPP-4M
1998

More Jet-like cells

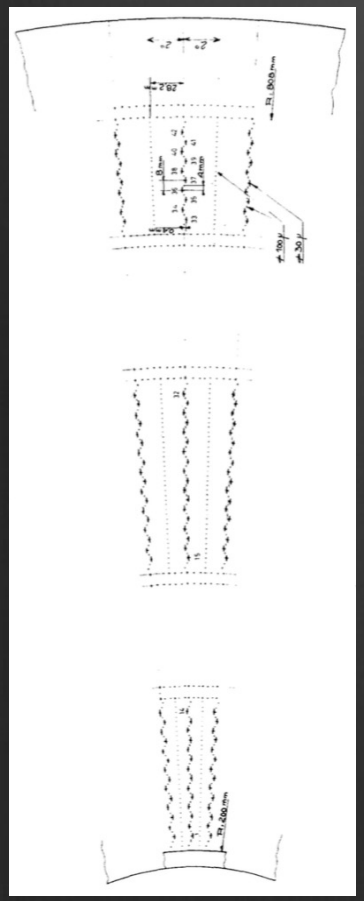

5.625:1
AFS
ISR
1982

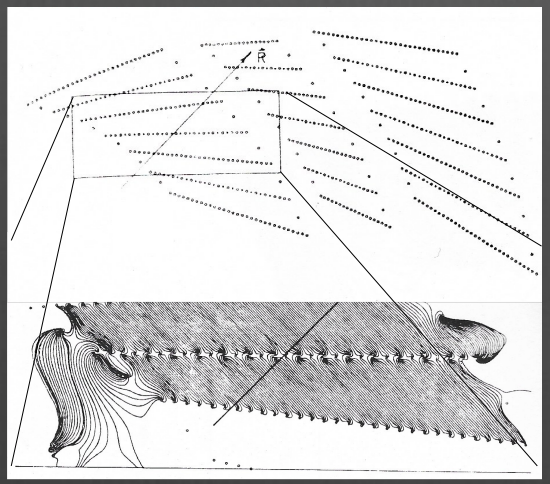

4.9:1
CDF CTC
Tevatron
1988

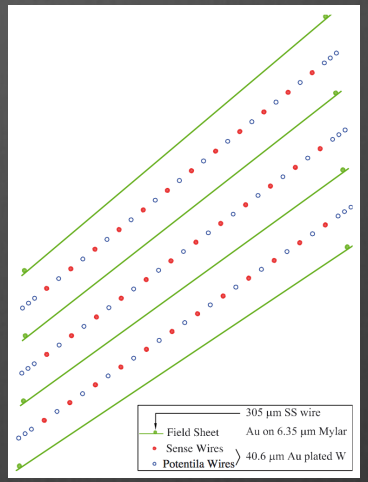

CDF COT
Tevatron
2002

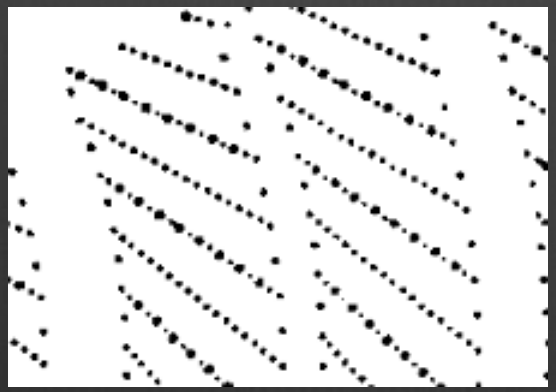

4.25:1
ZEUS
HERA
1992

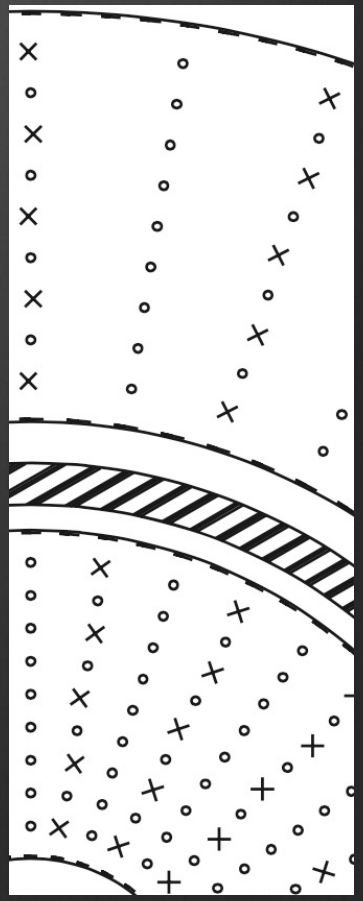

2.6:1
SND
VEPP-2M
1995

Multi-wire and Jet-like cells Layout

	MARK3 SPEAR (1980)	JADE PETRA (1980)	CMD-2 VEPP-2M (1985)	MARK2 PEP/SLC (1985)	SLD SLC (1988)	OPAL LEP (1988)	BES/BESII BEPC (1989)	KEDR VEPP-4M (1998)
Inner Radius [mm]	140	180	25	192	200	245	155	125
Outer Radius [mm]	1140	800	295	1519	1000	1850	1150	535
Length [mm]	2337	2400	440	2300	2000	4000	2200	1100
Axial layers	12+4×3	16×2	6+7+6	6×6	4×8	159×1	5×4	4×6
Stereo layers	2×3	0	0	6×6	6×8	0	5×4	3×6
Stereo angles [mrad]	±150	0	0	±66	±41	0		±52
Number of sense wires	2000	1536	512	5832	5300	3816	2808	1512
Total number of wires	6,240	3360	3,500	37,000	35,000	20,000	19,400	16,000
sense wires [μm]	20 W(Au)/57 SS	25 W-Re(Au)	25 Ni-Cr	30 W(Au)	25 W(Au)	25 W-Re	30 W	28 W(Au)
field wires [μm]	175 Cu-Be	125-175 Cu-Be	10-20 Ti(Cu)	178-305 Cu-Be(Au)	150 Al(Au)	125-175 Cu-Be	100-178-200 Cu-Be	70-150 Ti(Au)
Inner cylinder [mm/X_0]	9.5 HC+mylar+Al /0.2%			2.0 Be / 0.6%	Al + HC	1.5 C-f / 0.7%		1.5 C-f / 0.7%
Outer cylinder [mm/X_0]	6.25 Al / 7.0%			12.7 Al / 15.0%	Al + HC			5.0 G10 / 3.0%
End-plates [mm/X_0]	25.4 / 15% - 7.62 / 8.5%	25.4 G10 /15.0%	10.0 G10 / 6.0%	51.0 Al / 57.0%	5.0 Al / 5.7%	32 G10 / 19.2% / 28 Al /33.0%		20 G10 / 12.0%

Multi-wire and Jet-like cells Performance

	MARK3 SPEAR (1980)	JADE PETRA (1980)	CMD-2 VEPP2M (1985)	MARK2 PEP/SLC (1985)	SLD SLC (1988)	OPAL LEP (1988)	BES/BESII BEPC (1989)	KEDR VEPP4M 1998)
B-field [T]	0.4	0.45	2.0	0.4	0.6	0.44	0.4	0.6 (1.8)
Cell Size [mm²]	(18÷30)×10	(10÷30)×10	(16÷28)×10	33×8.33	60×50	(30÷250)×10	30×10	30×4.5
Gas Mixture	HRS gas	88.7 Ar / 8.5 CH_4 / 2.8 iC_4H_{10}	80 Ar / 20 iC_4H_{10}	HRS gas	21 Ar / 72 CO_2 / 4 iC_4H_{10}	88 Ar / 10 CH_4 / 2 iC_4H_{10} at 4 bar	HRS gas	C_2H_2O (DME)
Spatial Resolution [μm]	220	135-165	95	175	155	135	240	115
Momentum Resolution	0.015p / 0.015	0.022p / ?	? / ?	0.0015p /0.014	0.010p / 0.005	0.00150p / 0.02	0.018p / 0.018	0.02p / 0.03
Δp [MeV/c] at 1 GeV/c	21	>22	50	14.1	11.1	20	25	36
dE/dx	15.0%	6.0% - 8.5%	//	7.0%	6.4%	3.1% - 3.8%	8.5%	8.5%

Lesson #2 - from single to multi-wire

- left-right ambiguity solved at the cell level
- track finding facilitated by the definition of a point and a vector within a single cell
- double track resolution improved with suitable front-end electronics

... but

- very long drift times
- portions of active volume not sampled between the cylindrical envelope of axial wires and the hyperboloid envelope of stereo wires
- need for extra (thick) wires to limit cross-talk between adjacent sense wires and for extra wires at cell boundary to limit long drifts
- only limited stereo angles allowed because of its radial dependence for long jet-like cells

Momentum resolution in early chambers

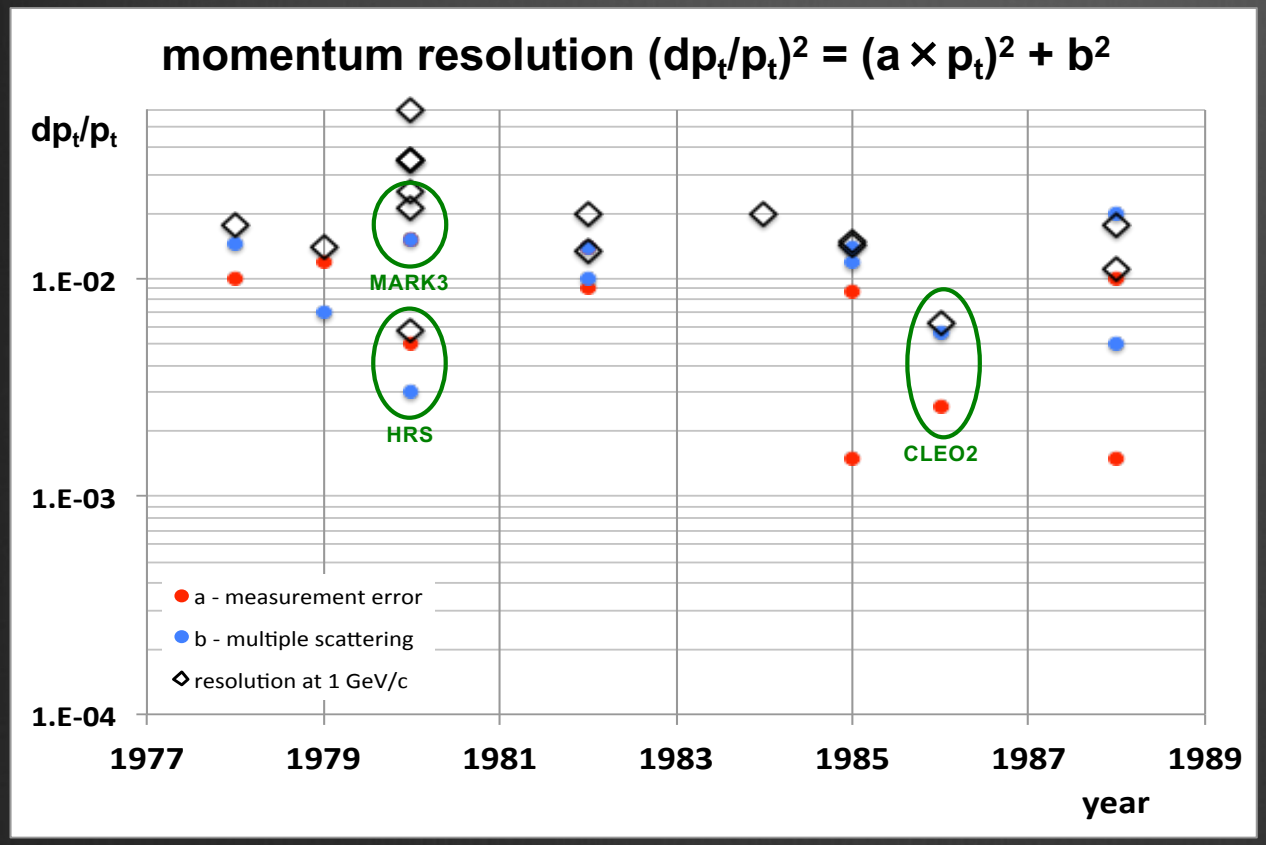

$$(dp_t/p_t)^2 = [8\sqrt{5}\sigma_{r\varphi}/(0.3BL^2\sqrt{N})]^2 p_t^2 + [5.4 \times 10^{-2}/BL\sqrt{(L/X_0)}]^2$$

Despite the large variety of different parameters involved, **momentum resolution** (at p=1GeV/c) clusters around **1-2%** for all chambers.

Initially, resolution dominated by the sagitta measurement error. With improved cell configurations, the dominant error became multiple scattering, claiming for a **breakthrough** in the **gas mixture** and in the **wires**.

Helium as Drift Chamber gas ...

W. Zimmermann et al., *Helium-propane as drift chamber gas*, Nucl. Instrum. Meth. A243 (1986) 86

F. Grancagnolo, *A Helium Drift Chamber as the Central Tracker of a B-Factory*, Proc. Workshop on Heavy Quarks Factory and Nuclear Physics Facility with Superconducting Linacs, Courmayeur, 1987, eds. E. De Sanctis, M. Greco, M. Piccolo and S. Tazzari (Atti di Coferenze, Società Italiana di Fisica, Bologna 1987) p. 599

F. Grancagnolo, *A Central Tracking Detector for a B-Factory*, Nucl. Instrum. Meth. A277 (1989) 110

... and back to single sense wire cells

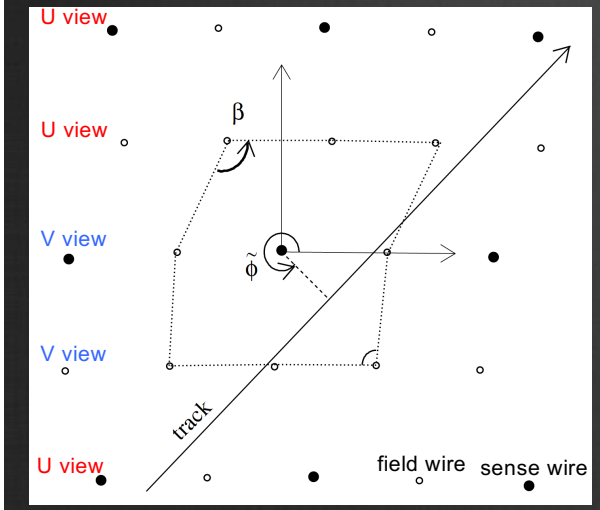

KLOE

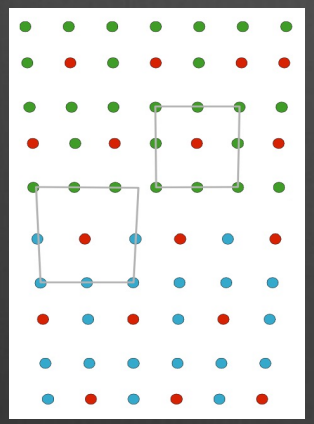

CLEO3

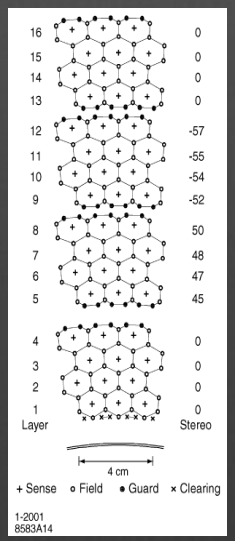

BABAR

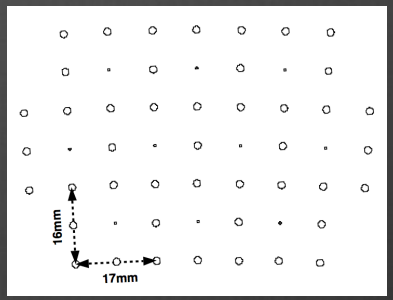

BELLE

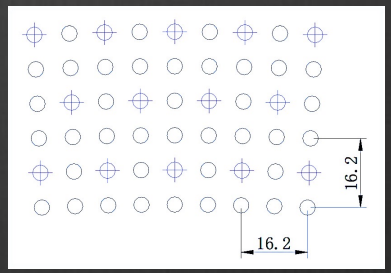

BES3

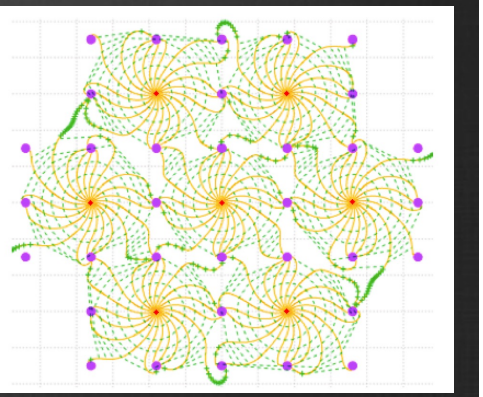

BELLE2

Single wire cells – He gas Layout

	BESIII BEPC2 (2008)	KLOE DAPHNE (1998)	CLEO3 CESR2 (1998)	BABAR PEP2 (1998)	BELLE KEKB (1998)	BELLE2 KEKB (2017)
Inner Radius [mm]	63	250	125	236	77	160
Outer Radius [mm]	810	1980	820	808	880	1130
Length [mm]	2400	3300	2500	2800	2400	2420
Axial layers	5×4	0	8×2	4×4	6×5	5×6
Stereo layers	6×4	12+46	8×4	6×4	5×4	4×6
Stereo angles [mrad]	±35÷50	±60÷150	±20÷30		±42÷74	±60÷80
Number of sense wires	7000	12582	9796	7104	8400	14,336
Total number of wires	29,000	52,000	40,000	25,000	35,000	60,000
sense wires [μm]	25 W-Re(Au)	25 W(Au)	20 W-Re(Au)	20 W-Re(Au)	30W(Au)	30 W(Au)
field wires [μm]	110 Al(Au)	80 Al(Ag)	110 Al(Au)	80-120 Al(Au)	126 Al	126 Al
Inner cylinder [mm/X_0]	1.0 C-f / 0.45%	0.75 C-f + 0.2 Al / 0.55%	2.0 Roh + Al / 0.12%	1.0 Be / 0.28%	2.0 C-f / 1.1%	0.4 C-f / 0.22%
Outer cylinder [mm/X_0]	11.0 C-f / 5.0%	3.0 C-f + HC / 2.5%		C-f + HC / 1.5%	5.0 C-f / 2.6%	5.0 C-f / 2.6%
End-plates [mm/X_0]	25.0 Al / 28.0%	9.0 C-f / 4.7%	15.5 Al + ... / 17%	12/24 Al / 13.5%/27.0%	10.0 Al / 11.0%	10.0 Al / 11.0%

Single wire cells – He gas Performance

	BESIII BEPC2 (2008)	KLOE DAPHNE (1998)	CLEO3 CESR2 (1998)	BABAR PEP2 (1998)	BELLE KEKB (1998)	BELLE2 KEKB (2017)
B-field [T]	1.0	0.6	1.5	1.5	1.5	1.5
Cell Size [mm²]	12×12 ÷ 16×16	20×21 + 30×31.5	14×14	12×18	8×15.5 + 10×17	87.5 + 15,25
Gas Mixture	60 He / 40 C_2H_6	90 He / 10 iC_4H_{10}	60 He / 40 C_2H_6	80 He / 20 iC_4H_{10}	50 He / 50 C_2H_6	50 He / 50 C_2H_6
Spatial Resolution [μm]	120	200	110	125	130	130
Momentum Resolution	0.0032p / 0.0037	0.0005 / 0.0026	0.0016p /0.0028	0.0015p / 0.0045	0.0019p / 0.0030	0.0011p / 0.0025
Δp [MeV/c] at 1 GeV/c	4.9	2.6	3.2	4.7	3.5	2.7
dE/dx	6%-7%	4.6%	5.0%	7.5%	6.9%	6.9%

Lesson #3 – small cells and He gas

- He radiation length 50 × longer than Ar
- slower drift velocity implies smaller Lorenz angle for a given B-field
- He has a smaller cross section for low energy photons than Ar
- small size cells limit the electron diffusion contribution to spatial resolution
- small size cells provide high granularity (improving occupancy) and allow for a larger number of hits per track, improving spatial resolution

... but

- portions of active volume not sampled between the cylindrical envelope of axial wires and the hyperboloid envelope of stereo wires
- accumulation of trapped electrons and ions in a region of very low field
- longitudinal gain variation at boundaries between axial and stereo layers
- spatial resolution dominated by ionization statistics for short drift distances
- adding more quencher to compensate, mitigates the advantage of He

p_t resolution after He

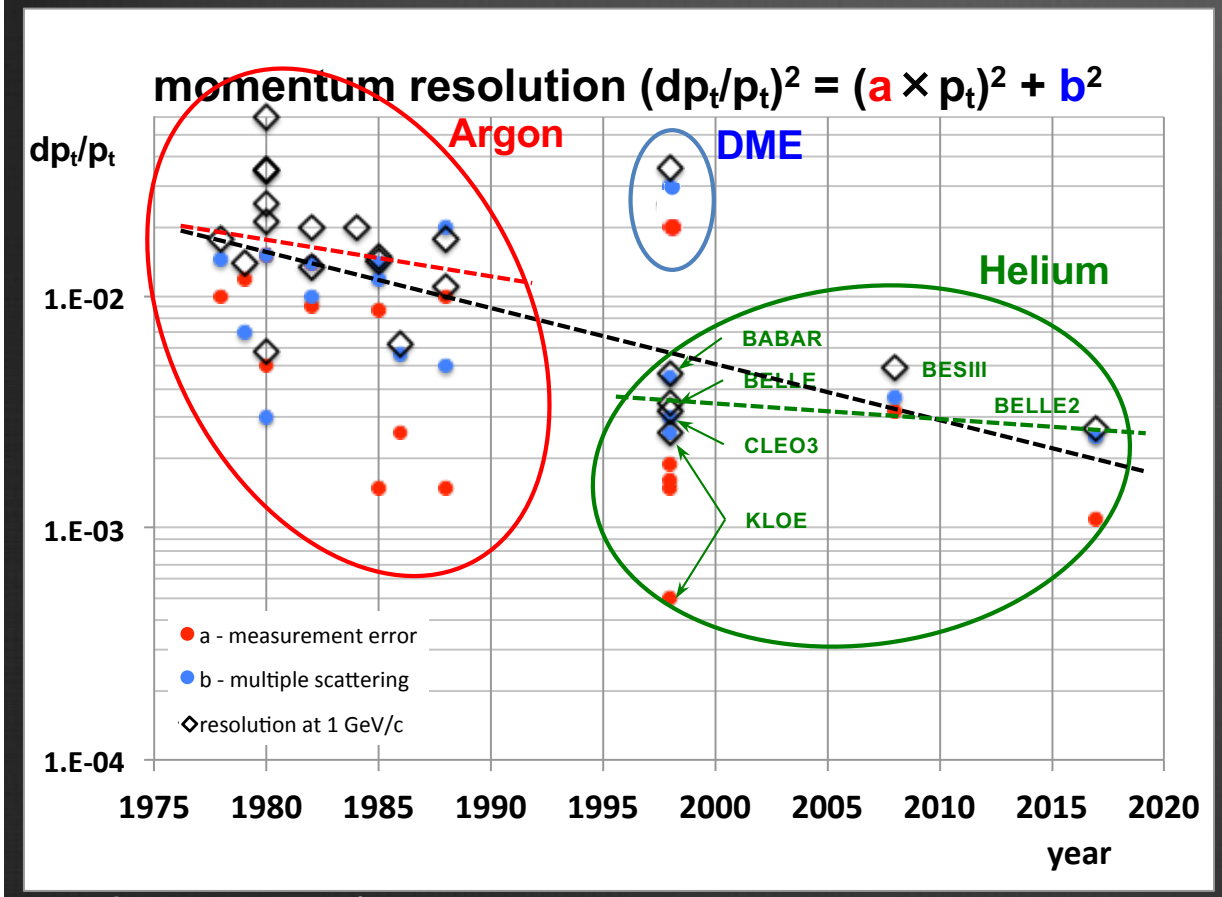

$$(dp_t/p_t)^2 = [8\sqrt{5}\sigma_{r\varphi}/(0.3BL^2\sqrt{N})]^2 p_t^2 +$$
$$+ [5.4 \times 10^{-2}/BL\sqrt{(L/X_0)}]^2$$

from

1-2% (in Ar)

to

few $\times 10^{-3}$ (in He)

"Full" stereo configuration: KLOE

A configuration with only perfectly nested alternating sign stereo layers (no axial layer) fills the gaps occurring in a mixed stereo-axial configuration, rendering the chamber more isotropic and fully sampled, thus maximizing the number of hits on a track for a given cell size.

In **KLOE**, this is achieved by having the field wires layer of the cell outer bound at a stereo angle of opposite sign w.r.t. the sense wire layer and to the field wires layer of the cell inner bound

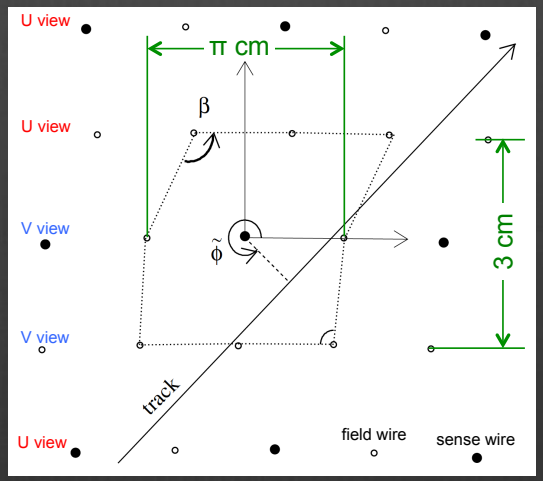

The stereo configuration is obtained with constant stereo drop at the middle transverse plane. This, however, besides causing a small longitudinal variation of the cell aspect ratio, implies:
time to distance relations which depend on the track angle and on the cell periodicity in z.

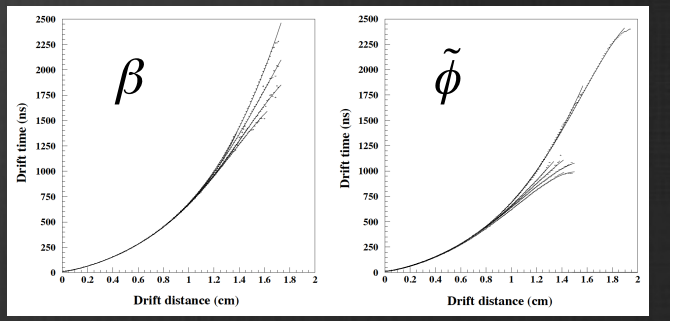

Lesson #4 – full stereo configuration

- no gaps between axial and stereo layers which may trap ions and electrons in regions of very low electric field
- constant sense wire gain as a function of the longitudinal coordinate
- larger number of hits on a track for a given cell size
- maximizes the number of measurements of the longitudinal coordinate
- two stereo views enable 3D reconstruction in a natural way

... but

- open top cells cause a dependence of the time-to-distance relations from the track angle and from the cell longitudinal periodicity
- constant stereo drop (as in KLOE) changes the cell aspect ratio along z (radial cell size constant but azimuthal width increased at end-plates)
- constant stereo angle generates cell distortions for large stereo angles

MEG2 approach at "full" stereo

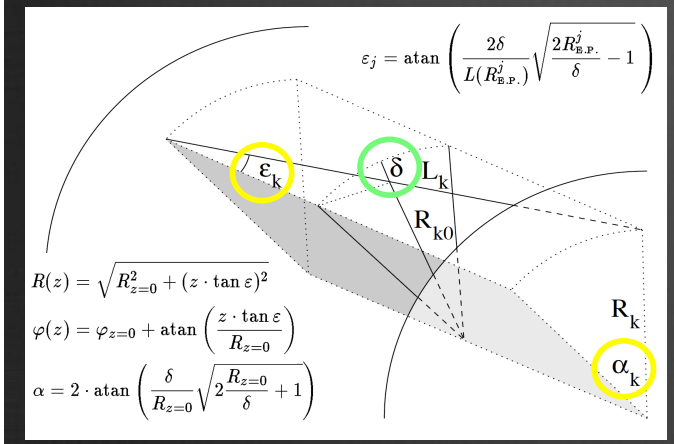

Constant transverse stereo angle projection α_k preserves the cell aspect ratio:
"square" cells by construction: $w_k = h_k$ remain such at any z
[$w_k(z=\pm L/2) = h_k(z=\pm L/2) = 1.035\ w_k(z=0) = 1.035\ h_k(z=0)$ for 100 mrad stereo angle and 2 m wire length]
no β angle dependence - no Φ angle dependence
in principle, one single t-to-d scalable for all layers

Layer assembly

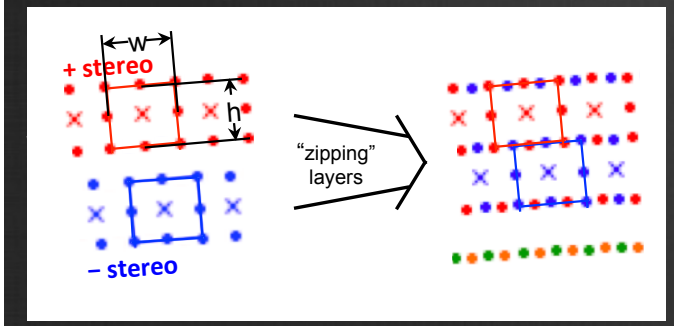

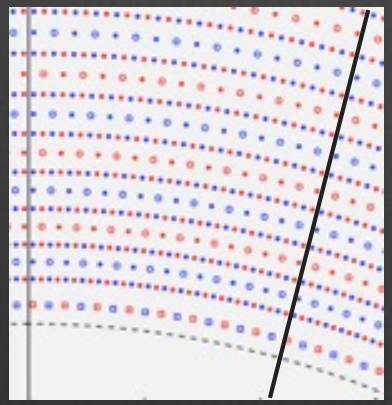

This configuration requires more field wires per sense wire (5:1, as opposed to 3:1 in KLOE) allowing for thinner field wires, therefore, even less m.s. contribution and less load on the end plates.

Lesson #5 – summary

- the configuration offering the best performance in terms of **momentum and angular resolutions** is the one with small, single sense wire closed cells, arranged in contiguous layers of opposite sign stereo angles, obtained with constant stereo angle transverse projection
- the gas mixture is based on helium with a small amount of quencher (90% He / 10% iC_4H_{10}, KLOE gas) which, besides the low multiple scattering contribution, allows for the exploitation of the cluster timing technique, for improved spatial resolution, and of the cluster counting technique, for excellent particle identification
- suggested wire material is Ag coated Al, but lighter materials are under scrutiny (like metal coated carbon monofilaments)

PId with dE/dx: the task

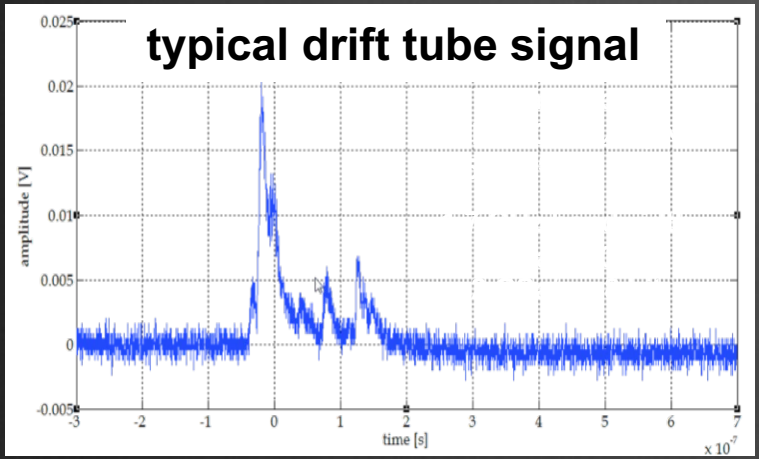

By definition, **the integral** of this signal is proportional to the **total number of electrons** liberated in the ionization process which, in turn, is proportional to the **energy lost** by the charged particle crossing the **dx** layer of gas (**− dE/dx**).
By knowing the dependence of dE/dx form the velocity **β** of the crossing particle, given **p**, one can identify the particle **mass**.

Also, the **theory model description of the energy loss mechanism** needs to be accurate **at 1% level**

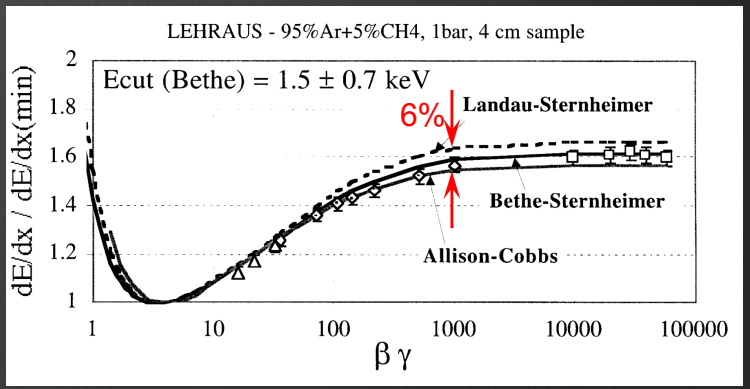

J. Va'vra *Particle Identification Methods in High Energy Physics,* **SLAC-PUB-8356, Jan. 2000**

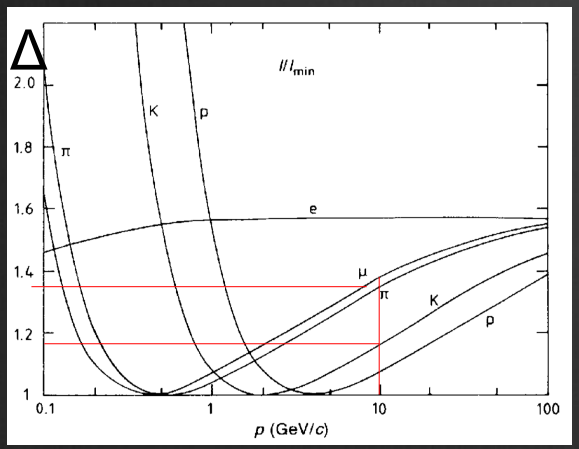

In the relativistic rise region:
[Δ(π) – Δ(K)] / Δ(π) ≈ 10-15%
π/K separation requires **resolutions δΔ/Δ** of **better than a few %**

PId with dE/dx: the straggling function

Definitions and iterative application of convolution integral

$d\sigma(E,\beta)/dE$ collision cross section for an energy transfer **E** by a particle of velocity **β**

$\lambda = \lambda(\beta) = 1/(n_e\sigma)$ mean free path between collisions (n_e = linear density of electrons)

$N_c = x/\lambda$ mean number of collisions over a length **x**

Bichsel et al., Phys. Rev. A 11, 1286 (1975)

$F_{(1)}(E) = 1/\sigma\ d\sigma(E,\beta)/dE = n_e\lambda\ d\sigma(E,\beta)/dE$ probability to transfer energy **E** in a single collision

$F_{(k)}(\Delta) = \int_0^{\Delta} F_{(1)}(E)\ F_{(k-1)}(\Delta-E)\ dE$ probability to transfer energy **Δ** in **k** collisions
k-fold convolution of $F_{(1)}(E)$

$P(k, N_c) = N_c^k/k!\ \exp(-N_c)$ probability of **k** collisions with mean **N_c** (Poisson)

$f(\Delta,x) = \sum_{k=0}^{\infty} P(k, N_c)\ F_{(k)}(\Delta)$ probability density function for energy loss **Δ** over **x**
straggling function

PId with dE/dx: the straggling function

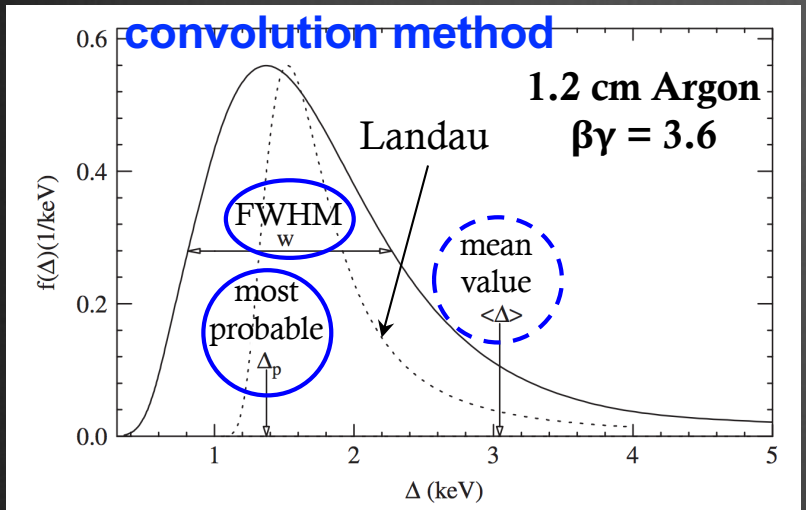

Fig. 1. The straggling function $f(\Delta)$ for particles with $\beta\gamma = 3.6$ traversing 1.2 cm of Ar gas is given by the solid line. It extends beyond $E_{max} \sim 2\,mc^2\beta^2\gamma^2 = 13$ MeV. The original Landau function [2,3] is given by the dotted line. Parameters describing $f(\Delta)$ are the most probable energy loss $\Delta_p(x;\beta\gamma)$, i.e. the position of the maximum of the straggling function, at 1371 eV, and the full-width-at-half-maximum (FWHM) $w(x;\beta\gamma) = 1463$ eV. The mean energy loss is $\langle\Delta\rangle = 3044$ eV.

for a rigorous treatment see:

H. Bichsel, *A method to improve tracking and particle identification in TPCs and silicon detectors,* **NIM A562 (2006) 154**

parameters describing the straggling function: most probable energy loss:

$\Delta_p(x,\beta\gamma)$

and FWHM:

$W(x,\beta\gamma)$

There exist several different approaches to calculate the energy loss distribution (**the straggling function**) besides the convolution method (iterative application of convolution integral):

- **Laplace transform** method*
- **Monte Carlo method****
- **empirical fit to data*****

and a plethora of different models based on different parameterization of the collision cross section **σ** with *ad-hoc* corrections

*L. Landau, J. Phys. USSR 8, 201 (1944)

**Cobb et al., Nucl. Instr. Meth. 133, 315 (1976)

***Blum, Riegler, Rolandi, Springer-Verlag 2008
doi: 10.1007/978-3-540-76684-1 10

PId with dE/dx: the straggling function

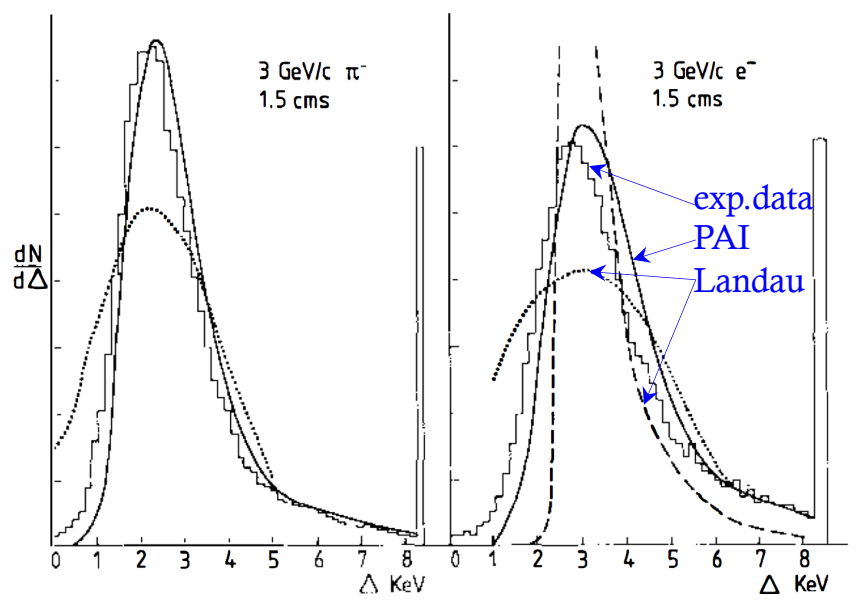

Figure 9 Experimental energy-loss distributions of Harris et al (1973) for π and e at 3 GeV/c in 1.5 cm of argon/7% CH_4 at normal density. The dashed and dotted curves are calculations using the model of Landau (1944) with corrections of Maccabee & Papworth (1969) and Blunck & Leisegang (1950) respectively. The solid curves are the predictions of the PAI model.

W. Allison and J. Cobb, *Relativistic charged particles identification by energy loss,* **Ann. Rev. Nucl. Part. Sci. 1980. 30: 253-98**

comparison with data

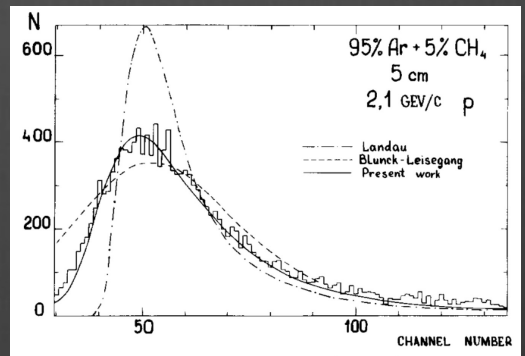

Fig. 4. The energy loss distributions for 2.1 GeV/c protons (near ionization minimum) in 5 cm of a mixture of Ar (95%) and CH_4 (5%). The histogram is obtained in the experiment by Kopot et al.[13]). The smooth curves are calculated for 5 cm of Ar at NTP without correction for detector resolution. The dash–dotted, dashed and solid curves are Landau, Blunck–Leisegang distributions and present work results respectively. Experimental and calculated data are normalised to the same Δ_{mp}.

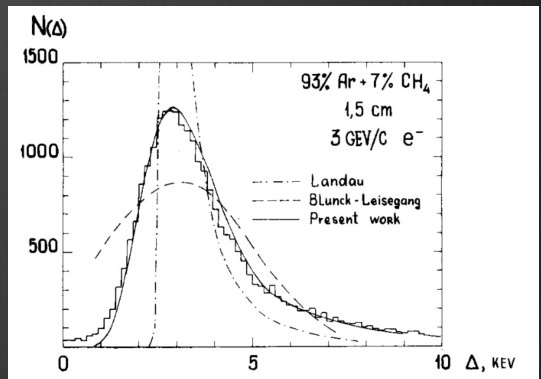

Fig. 5. The energy loss distribution for 3 GeV/c electrons (Fermi plateau region) in 1.5 cm of a mixture of Ar (93%) and CH_4(7%). The histogram is taken from a paper by Harris et al.[9]). The smooth curves are calculated for 1.5 cm of Ar at NTP without correction for detector resolution. The dash–dotted, dashed and solid curves are Landau, Blunck–Leisegang predictions and present work results respectively.

V. Ermilova, L. Kotenko, G. Merzon, *Fluctuations and the most probable values of relativistic charged particle energy loss in thin gas layers,* **NIM 145 (1977) 555**

The Maximum Likelihood measurement

- The energy loss distribution (straggling function) **f(Δ)** for a single sample is made of **a broad peak** due to low energy transfer **(soft) collisions** with the gas molecules and **a long tail** due to large energy transfer **(hard) collisions** which cause the release of **more than one electron** and/or **δ rays**.
- Typical **FWHM** of the energy loss distribution is in the range of **60-100% Δ_p** (very slowly dependent from βγ – except for very small sample lengths), which makes necessary to measure many samples (**n**) along the ionizing track in order to get a good enough estimate of the energy loss.

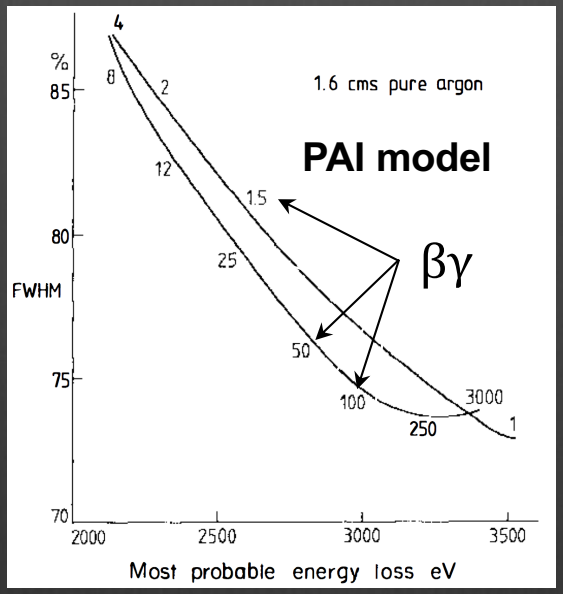

- With the assumption that the shape of the straggling function doesn't depend on βγ, one can construct a **likelihood function**:

$$L(\lambda) = \prod_{i=1}^{n} f(\Delta_i/\lambda).$$

The λ_0 (with its error $\delta(\lambda_0)$) which maximizes **L(λ)** is normally distributed and represents **the measured value of the most probable energy loss by the track under scrutiny**.
The mass assignment may then be calculated by comparing the expected ionization with λ_0 and $\delta(\lambda_0)$ using **normal error statistics**.

W. Allison and J. Cobb, Ann. Rev. Nucl. Part. Sci. 1980. 30: 253-98

The Truncated Mean measurement

- A much simpler and more robust procedure for obtaining analogous results is the method of **truncated mean**.
- It consists in cutting out a fraction **$(1-\eta)\cdot n$** of the largest **Δ_i** samples and extending the arithmetic mean to the remaining **$\eta\cdot n$** values (**m** is the closest integer to $\eta\cdot n$):

$$\langle\Delta\rangle_\eta = 1/m \sum_{j=1}^{m} \Delta_j \qquad \Delta_j \le \Delta_{j+1} \quad \text{for } j = 1, \ldots, n-1$$

- It can be shown that the range of values of **η** which minimizes the relative fluctuations of **$\langle\Delta\rangle_\eta$** for **Argon** is **between 0.4 and 0.7** (**0.8 for Helium**). Moreover, the **$\langle\Delta\rangle_\eta$** distribution behaves like a **gaussian distribution.**
- This is equivalent to the maximum likelihood method with:

$$\langle\Delta\rangle_\eta \cong \lambda_0 \quad \text{and} \quad \sigma(\langle\Delta\rangle_\eta) \cong \delta(\lambda_0)$$

PId with dE/dx: alternative methods?

Besides the truncated arithmetic mean, are there other effective methods?

data from BES III

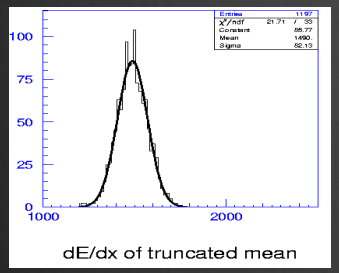

TM 70%

σ = 5.51%

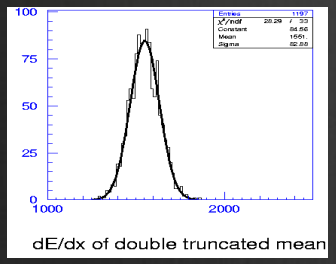

2TM 5-75%

σ = 5.34%

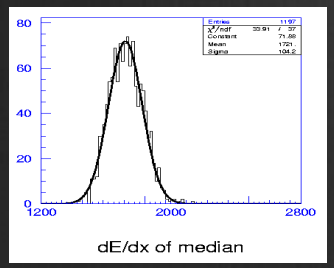

σ = 6.06%

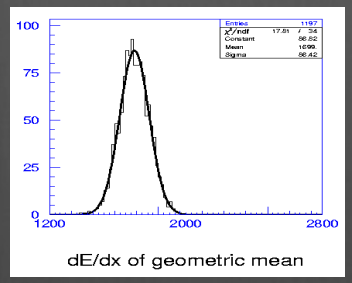

$$< \Delta >_g = \sqrt[n]{\prod_{i=1}^{n} \Delta_i}$$

σ = 5.09%

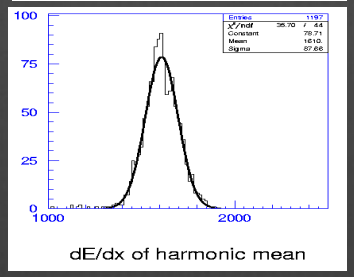

$$< \Delta >_h = \frac{n}{\sum_{i=1}^{n} 1/\Delta_i}$$

σ = 5.44%

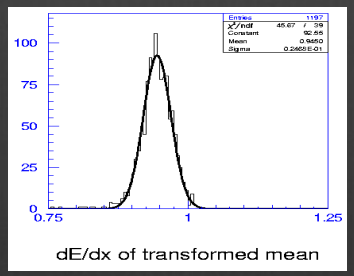

$$< \Delta >_t = \left(\sum_{i=1}^{n} \frac{1}{\sqrt{\Delta_i}} \right)^{-1}$$

σ = 2.61%

M. Hauschild, *Progress in dE/dx techniques used for particle identification* , **NIM A379(1996) 436**

PId with dE/dx: particle separation power

- The relevant quantity for discriminating between two different particles of masses **1** and **2** and momentum **p**, rather than λ_0 and $\delta(\lambda_0)$ for each of them, is:

$$D_{1,2}(p) = \frac{|\lambda_{0,1}(p) - \lambda_{0,2}(p)|}{[\sigma(\lambda_{0,1}) + \sigma(\lambda_{0,2})]/2}$$

separation measured in numbers of sigma

$$\sigma(\lambda_0) = \delta(\lambda_0)/\lambda_0$$

ALEPH TPC

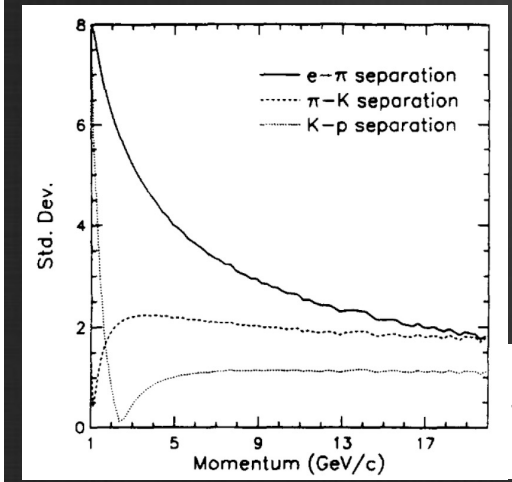

two-sided truncated mean: discard lowest 8% and largest 40%

$$\frac{\sigma_{dE/dx}}{(dE/dx)} = 4.5\%$$

OPAL Drift Chamber (4 bar)

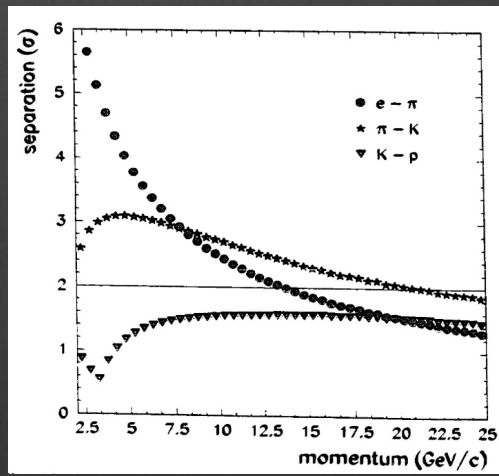

hit quality cuts and truncated mean: discard largest 30%

$$\frac{\sigma_{dE/dx}}{(dE/dx)} = \begin{matrix} 3.1\% \text{ (dimuons)} \\ 3.8\% \text{ (m.i.p.)} \end{matrix}$$

A few experimental facts for a PId detector

- The number of ionization acts follows the **Poison distribution** (≈10/cm/bar for He based, ≈30/cm/bar for Ar based gas mixtures)
- The number of electrons generated in each ionization act (**cluster size**) is subject to large fluctuations (*slide*)
- The accuracy of the ionization measurement depends on the mean free path between ionizing collisions **$\lambda = 1/(n_e\sigma)$** (i.e., on the collision cross section **σ** and on the electron number density **n_e**), therefore, on
  - the **gas mixture**;
  - the **sample length x** and its density, or the **gas pressure p** through their product **xp**;
  - the **number of samples n**, or, equivalently, the total length of the track **L = nx**.
- Empirical parameterization of resolution $\sigma(\lambda_0) = \delta(\lambda_0)/\lambda_0$ ([%] xp in [cm bar]) (*slide*):

$$\sigma(\lambda_0) = 41\ n^{-0.46}\,(xp)^{-0.32}\ [\%]$$

(for Argon) (based on ML, −0.46 → −0.43 with TM) Allison-Cobb Walenta

Number of electrons generated per cluster subject to large fluctuations

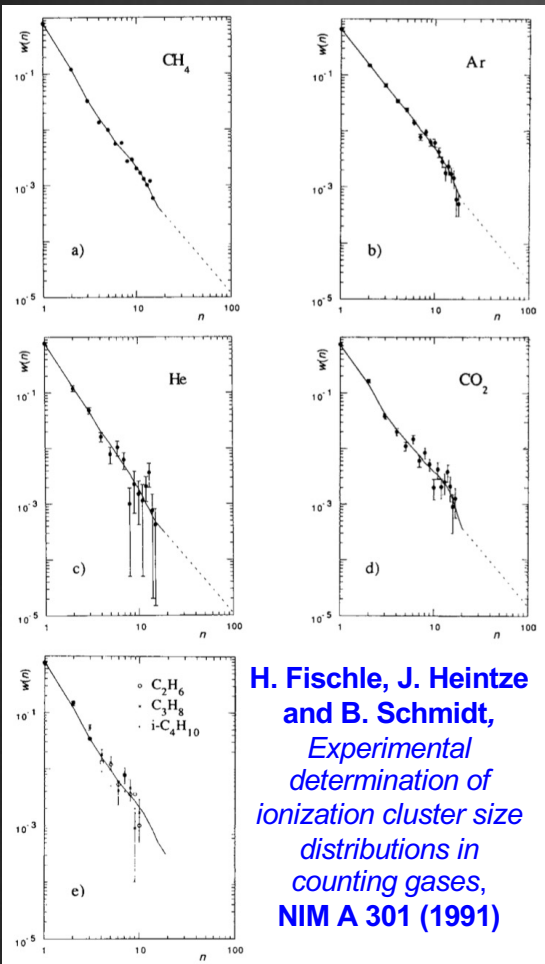

H. Fischle, J. Heintze and B. Schmidt, *Experimental determination of ionization cluster size distributions in counting gases,* **NIM A 301 (1991)**

	CH_4	Ar	He	CO_2
k				
1	78.6	65.6	76.60	72.50
2	12.0	15.0	12.50	14.00
3	3.4	6.4	4.60	4.20
4	1.6	3.5	2.0	2.20
5	0.95	2.25	1.2	1.40
6	0.60	1.55	0.75	1.00
7	0.44	1.05	0.50	0.75
8	0.34	0.81	0.36	0.55
9	0.27	0.61	0.25	0.46
10	0.21	0.49	0.19	0.38
11	0.17	0.39	0.14	0.34
12	0.13	0.30	0.10	0.28
13	0.10	0.25	0.08	0.24
14	0.08	0.20	0.06	0.20
15	0.06	0.16	0.048	0.16
16	(0.050)	0.12	(0.043)	0.12
17	(0.042)	0.095	(0.038)	0.09
18	(0.037)	0.075	(0.034)	(0.064)
19	(0.033)	(0.063)	(0.030)	(0.048)
≥ 20	$(11.9/k^2)$	$(21.6/k^2)$	$(10.9/k^2)$	$(14.9/k^2)$

HEED simulation
1 cm of He/iC_4H_{10} - 90/10

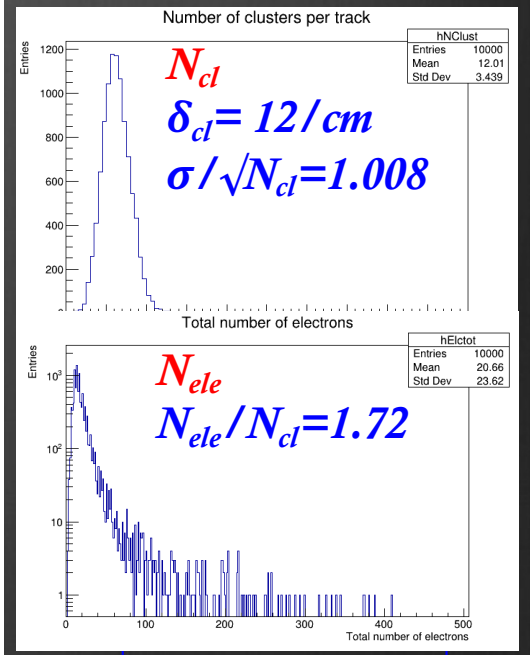

F. Cuna, G. Tassielli
private communication

notice the steeper distribution for **He** with respect to **Ar**

Parameterization of resolution $\sigma(\lambda_0)$

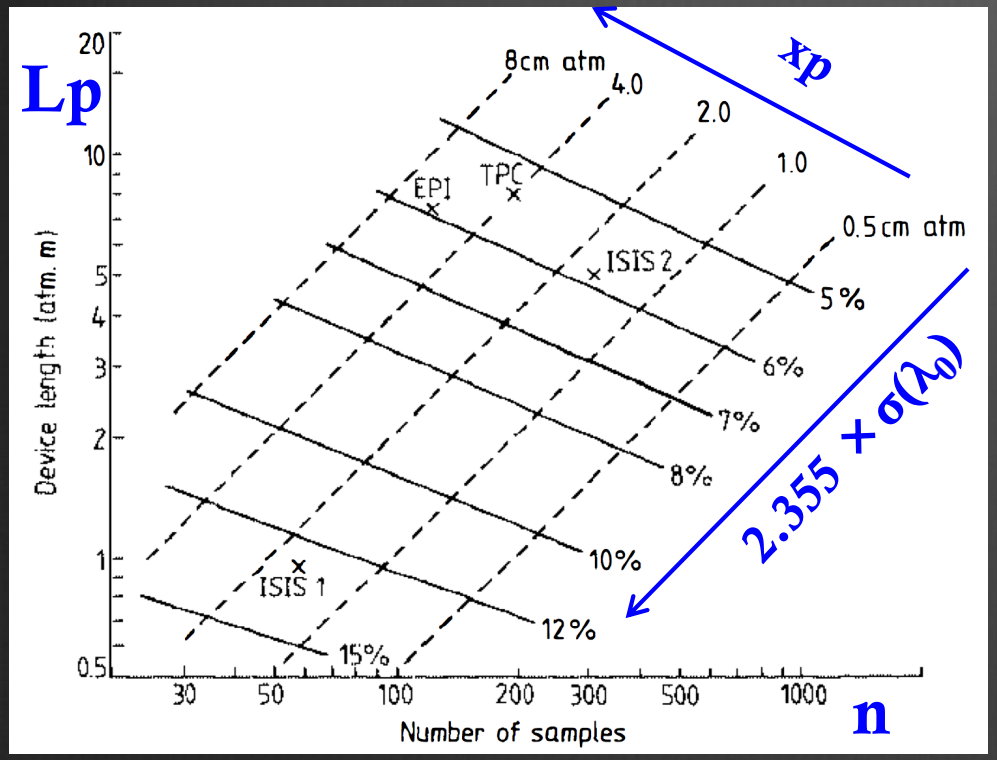

- keeping x fixed and increasing n or L improves the resolution
- keeping n fixed and varying L and x improves the resolution (*slide*)
- what is the optimal sample length for a fixed total length L?
  - the finer the better ($n^{-0.14}$)

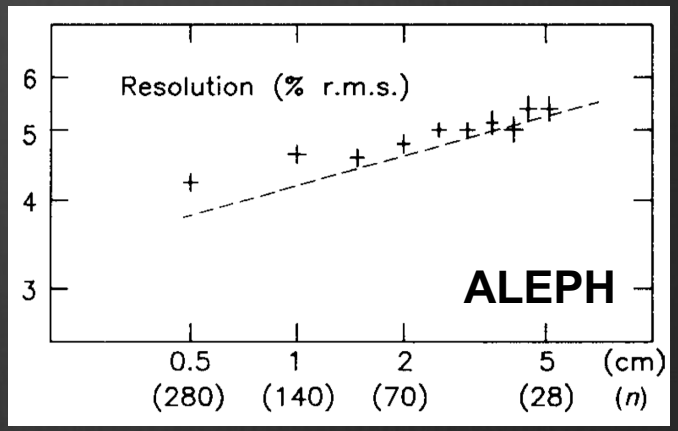

W. Allison and J. Cobb, *Relativistic charged particles identification by energy loss,* **Ann. Rev. Nucl. Part. Sci. 1980. 30: 253-98**

The average number of electrons per cluster increases with the sample length

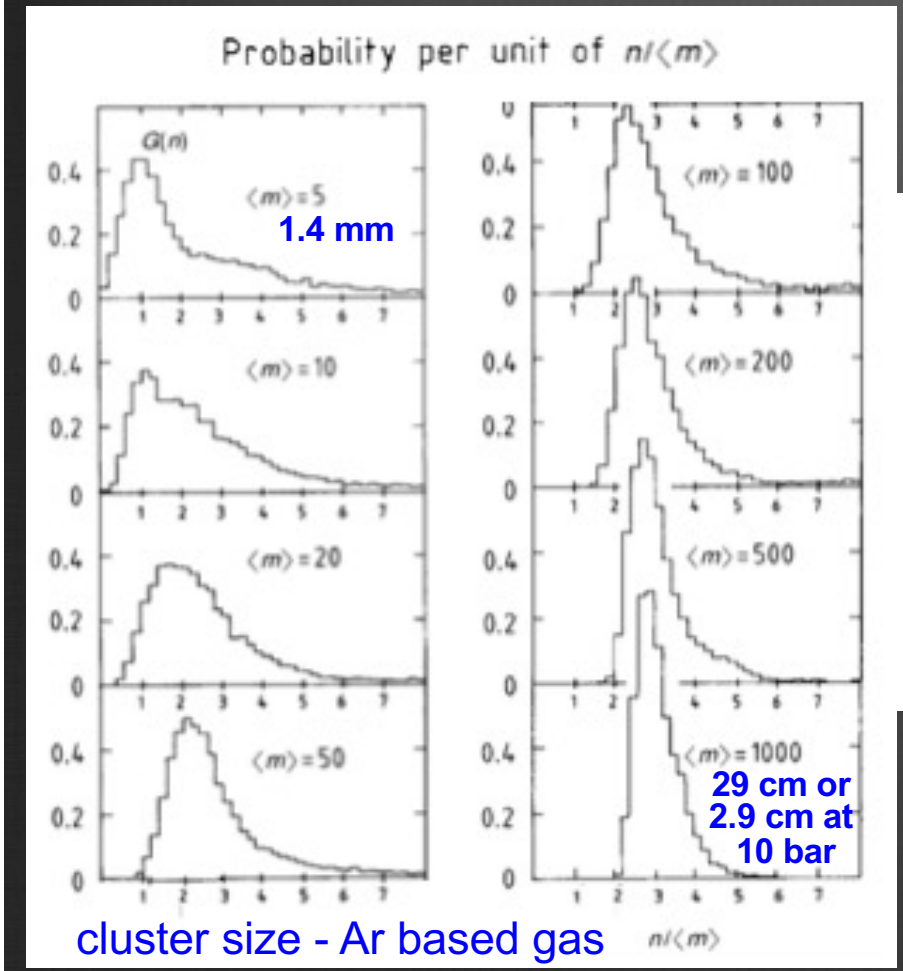

cluster size - Ar based gas

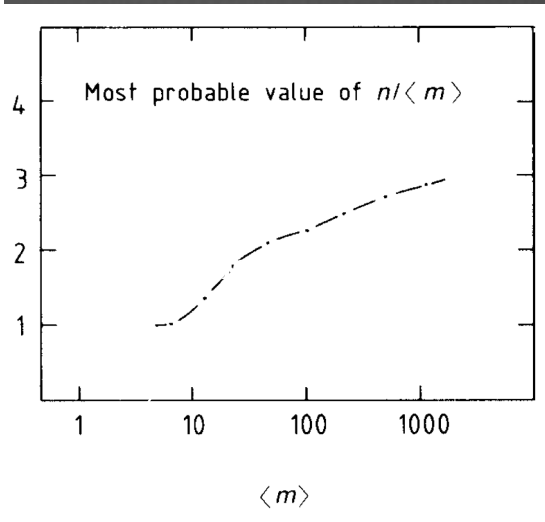

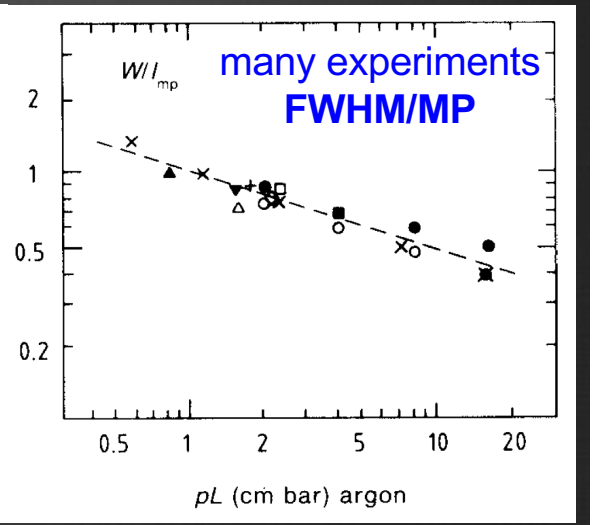

A.H. Walenta, *Performance and development of dE/dx counters,* **Phys. Scr. 23, 354 (1981)**

PId with dE/dx: gas choice

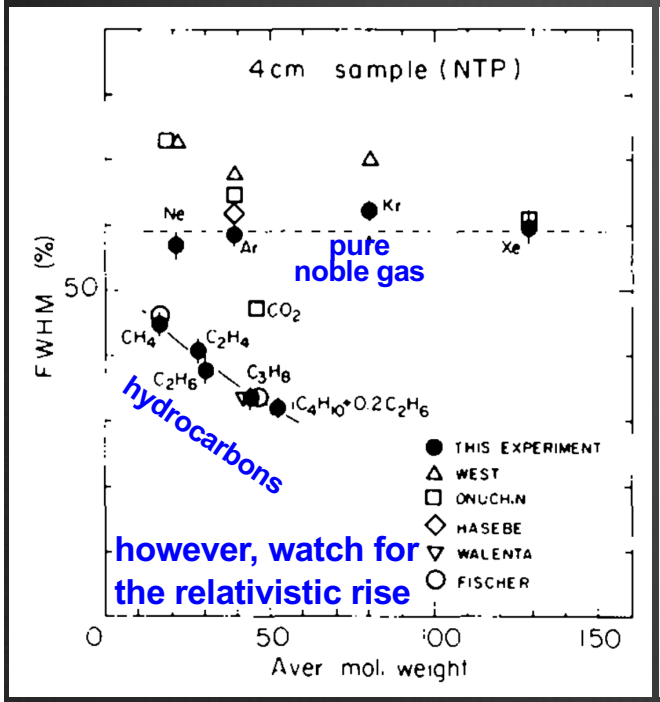

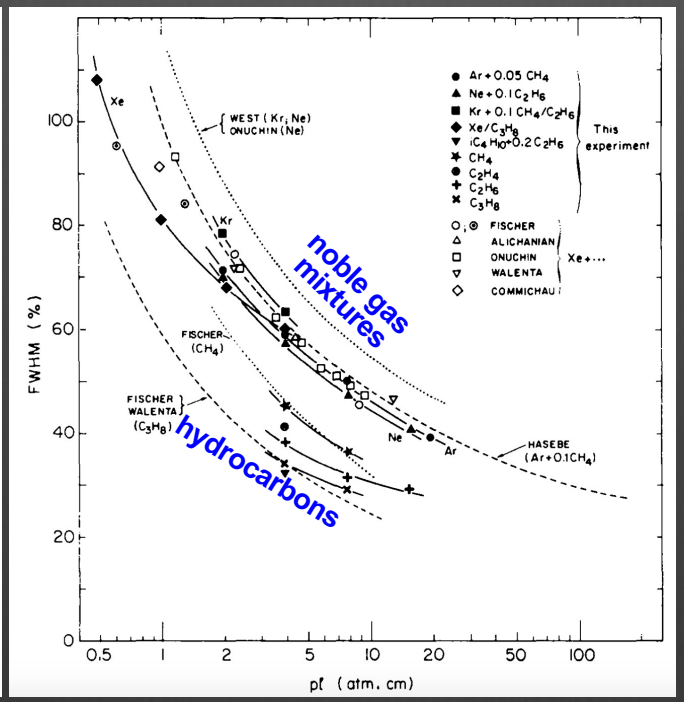

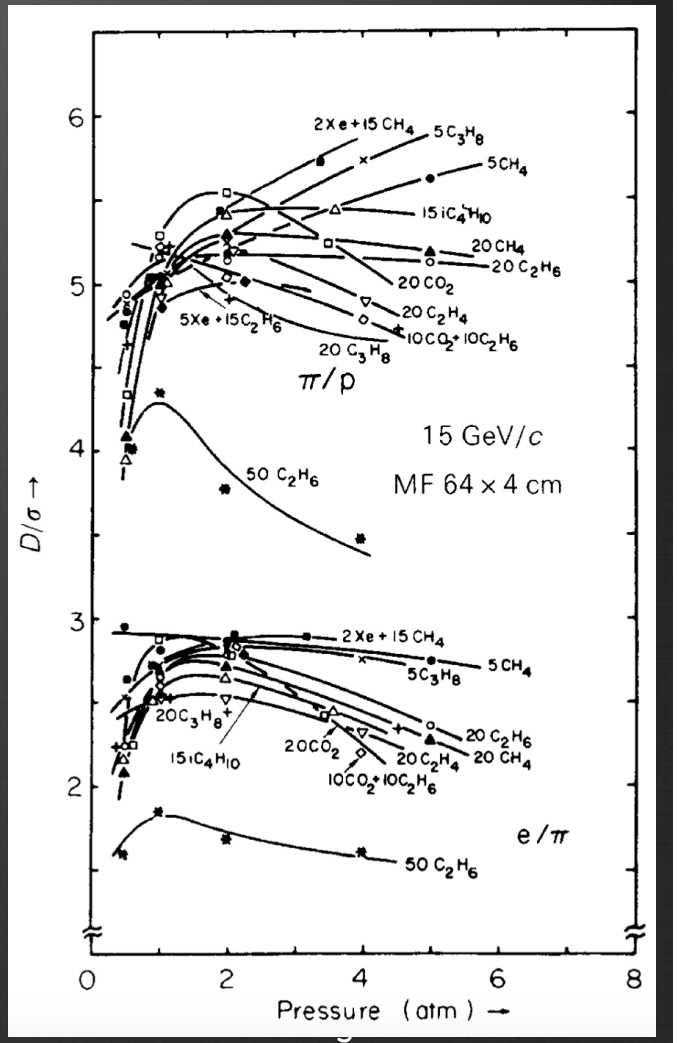

I. Lehraus, R. Mattewson and W. Tejesse, *dE/dx measurements in Ne, Ar, Kr, Xe and pure hydrocarbons,* **NIM 200 (1982) 199**

I. Lehraus, *Progress in particle identification by ionization sampling,* **NIM 217 (1983) 43**

dE/dx performance

from parameterization (slide 44)

Detector	Accelerator	Type	Size (Ø x L)	B (T)	Gas Mixture	Pressure (bar)	Number of samples	Sampling length (mm)	Effective track length (bar * m)	dE/dx resolution isol., dense (%)		Truncations (%)	Reference	
ALEPH	LEP	TPC	3.6 m x 4.4 m	1.5	Ar/CH_4 (91/9)	1	338	4	1.35	4.5		8-60	D. Buskulic et al., NIM A 360 (1995) 481	
ARGUS	DORIS	drift cells	1.7 m x 2 m	0.8	C_3H_8/Methylal	1	36	18	0.65	4.1	(4.4)	10-70	Y. Oku, PhD Thesis, Univ. of Lund (1985), LUNFD6/(NFFL-7024)/	
BaBar	PEP-II	drift cells	1.6 m x 2.8 m	1.5	$He/i\text{-}C_4H_{10}$ (80/20)	1	40	12	0.48	7.5		0-80	B. Aubert et al., NIM A 479 (2002) 1-116	
BELLE	KEK-B	drift cells	1.9 m x 2.2 m	1.5	He/C_2H_6 (50/50)	1	47	16	0.75	5.5	(7.0)	0-80	E. Nakano, NIM A 494 (2002) 402-408	6.0 +9%
BES	BEPC	jet cells	2.3 m x 2.1 m	0.4	$Ar/CO_2/CH_4$ (89/10/1)	1	54	5	0.27	9.0		0-70	J.Z. Bai et al., NIM A 344 (1994) 319	
CDF	TEVATRON	jet cells	2.6 m x 3.2 m	1.5	$Ar/C_2H_6/C_2H_6O$ (49.6/49.6/0.8)	1	32	12	0.38	7.0		?	D. Stuart, private communications	
CLEO II	CESR	drift cells	1.9 m x 1.9 m	1.5	Ar/C_2H_6 (50/50)	1	51	14	0.71	6.2	(7.1)	0-50	Y. Kubota et al., NIM A 320 (1992) 66	
CLEO III	CESR	drift cells	1.6 m x 1.9 m	1.5	He/C_3H_8 (60/40)	1	47	14	0.66	5.0		0-70	D. Peterson et al., NIM A 478 (2002) 142-146	6.3 +26%
CRISIS	TEVATRON	jet cells	1 m x 1 m x 3 m	-	Ar/CO_2 (80/20)	1	192	15	2.88	3.2		0-75	W.S. Toothacker et al., NIM A 273 (1988) 97	3.2 0%
DELPHI	LEP	TPC	2.4 m x 2.7 m	1.2	Ar/CH_4 (80/20)	1	192	4	0.77	5.7	(6.2)	0-80	P. Abreu et. al., CERN-PPE/95-194, submitted to NIM	
D0 FDC	TEVATRON	jet cells	1.2 m x 0.3 m	-	$Ar/CH_4/CO_2$ (93/4/3)	1	32	8	0.26	12.7		0-70	S. Rajagopalan, PhD Thesis, Northwestern University (1992)	
H1	HERA	jet cells	1.7 m x 2.2 m	1.13	Ar/C_2H_6 (50/50)	1	56	10	0.56	10.0		none*	I. Abt et al., NIM A 386 (1997) 348-396	
JADE	PETRA	jet cells	1.6 m x 2.4 m	0.48	$Ar/CH_4/i\text{-}C_4H_{10}$ (88.7/8.5/2.8)	4	48	10	1.92	6.5	(7.2)	5-70	K. Ambrus, PhD Thesis, Univ. of Heidelberg (1986)	
KEDR	VEPP-4M	jet cells	1.1 m x 1.1 m	2.0	DME (100)	1	42	10	0.42	10.0		5-70	S.E. Baru et al., NIM A 323 (1992) 151	
KLOE	DAΦNE	drift cells	4 m x 3.3 m	0.6	$He/i\text{-}C_4H_{10}$ (90/10)	1	58	28	1.62	3.5		0-80	A. Andryakov et al., NIM A 409 (1998) 390-394 (prototype)	4.5 +28%
MARK II	SLC	drift cells	3 m x 2.3 m	0.475	$Ar/CO_2/CH_4$ (89/10/1)	1	72	8.33	0.60	7.0		5-75	A. Bojarski et al., NIM A 283 (1989) 617	
NA49	SPS	TPC	3.8 m x 3.8 m x 1.3 m	-	$Ar/CH_4/CO_2$ (90/5/5)	1	90	40	3.60	4.7		10-65	B. Lasiuk, NIM A 409 (1998) 402-406	
OBELIX	LEAR	jet cells	1.6 m x 1.4 m	0.5	Ar/C_2H_6 (50/50)	1	40	15	0.60	12.0		0-70	F. Balestra et al., NIM A 323 (1992) 523	
OPAL	LEP	jet cells	3.6 m x 4 m	0.435	$Ar/CH_4/i\text{-}C_4H_{10}$ (88.2/9.8/2)	4	159	10	6.36	2.8	(3.2)	0-70	M. Hauschild, NIM A 379 (1996) 436.	2.6 -7%
SLD	SLC	jet cells	2 m x 2 m	0.6	$CO_2/Ar/i\text{-}C_4H_{10}$ (75/21/4)	1	80	6	0.48	7.0		?	M. Hildreth, private communications	
STAR	RHIC	TPC	4 m x 4.2 m	0.5	Ar/CH_4 (90/10)	1	45	17.2	0.77	8.0		0-70	M. Anderson et al., NIM A xxx (2003), in print	
TOPAZ	TRISTAN	TPC	2.4 m x 2.2 m	1.0	Ar/CH_4 (90/10)	3.5	175	4	2.45	4.4	(4.6)	0-65	M. Iwasaki et al., NIM A 365 (1995) 143	
TPC/2γ	PEP	TPC	2 m x 2 m	1.375	Ar/CH_4 (80/20)	8.5	183	4	6.22	3.0		0-65	G. Cowan, PhD Thesis, Lawrence Berkeley Lab. (1988), LBL-24715	2.5 -17%
ZEUS	HERA	jet cells	1.7 m x 2.4 m	1.43	$Ar/CO_2/C_2H_6$ (90/8/2)	1	72	8	0.58	8.5		?	W. Zeuner, private communications	

best performance — He based gas

* = inverse gaussian mean 1/sqrt[(dE/dx)i] used

Particle Identification Techniques with dE/dx — Michael Hauschild, 8th ICATPP, Como, 8-Oct-2003, page 26

Factors affecting uniform track signal response

Gas related factors

- composition (stability, pollutants)
- environmental parameters (pressure, temperature, ...)
- drift, gas gain, diffusion, space charge, attenuation

Geometry factors

- track angle
- cell geometry
- mechanical tolerances
- field uniformity

Electronics factors

- noise (white)
- coherent noise
- baseline stability
- threshold stability
- bandwidth
- electronic gain uniformity (calibrations)

W. Allison and P. Wright, *The Physics of Charged Particle Identification* **OUNP 35-83**

dE/dx resolution: current status

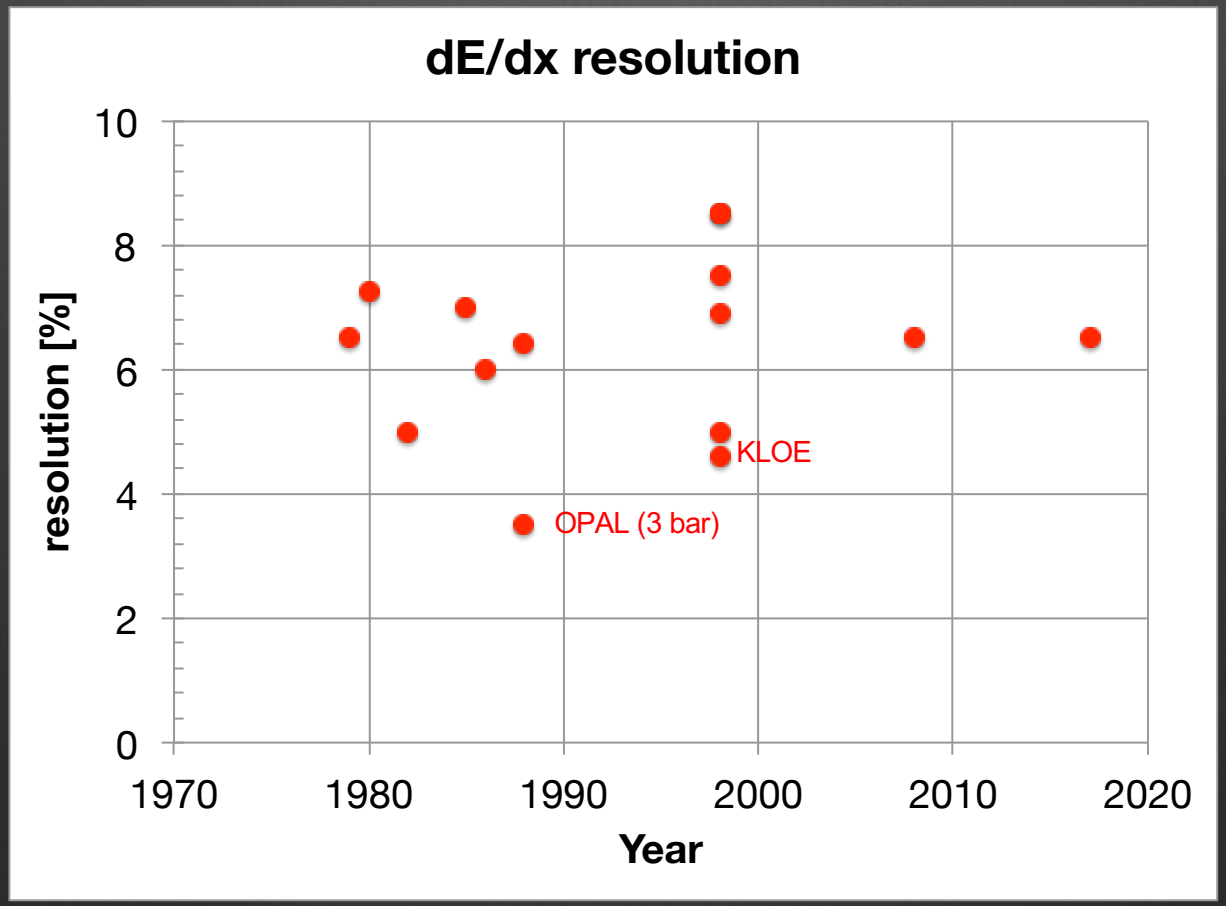

dE/dx comments and summary

- Methodology dates back to '80s. Very little progress in performance since then.
- Helium based gas mixtures, a priori disfavored because of the lower ionization statistics, compensate with fewer fluctuations and equal the Argon performance.
- However, much less documentation exists for dE/dx with Helium mixtures.
- Using the Allison-Cobb parameterization a **dE/dx resolution between 4.0% and 4.5%** (depending on geometrical constraints) is granted
- Given the very low He density, an increase in pressure might improve separation power (by 20% at 2 bar) without jeopardizing too much the momentum resolution (special PId dedicated runs?).
- A further 25% improvement may come at the expensive cost of a finer ($\times 2$) drift cell granularity.
- New techniques (ML?) might make the difference with respect to maximum likelihood and/or truncated mean methods, but do not expect miracles.
- Only a completely different approach, like **cluster counting**, may provide the necessary quantum leap.

PId with dN/dx: the task

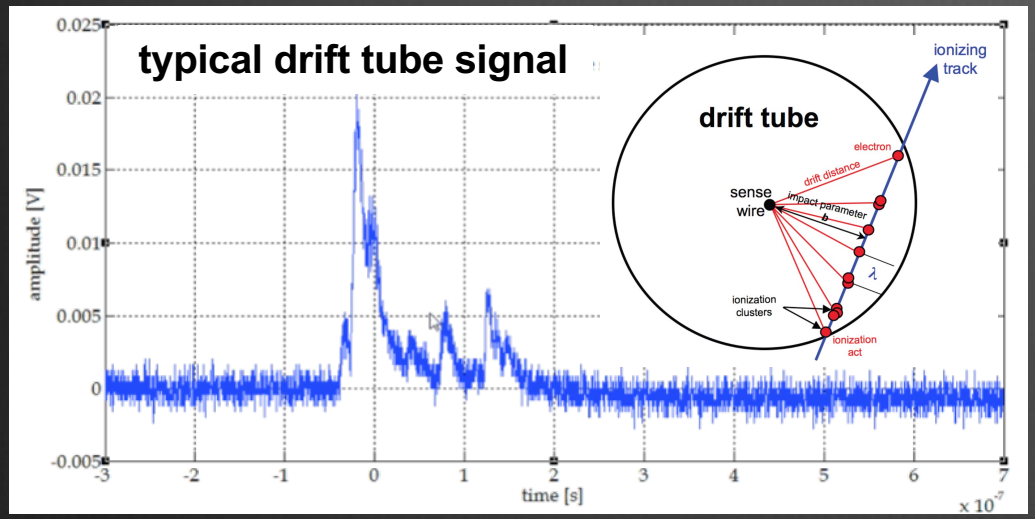

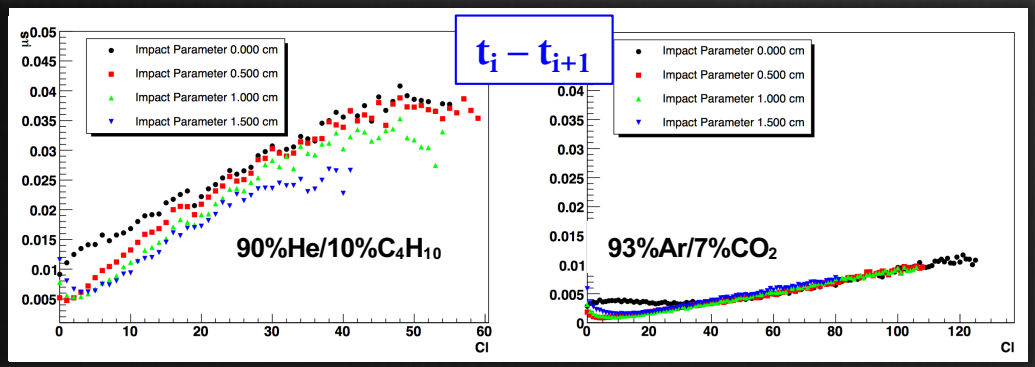

- **Cluster counting** consists in singling out, in every recorded detector signal, **the isolated structures related to the arrival at the anode wire of the electrons belonging to a single ionization act**.
- In order to achieve this goal, special experimental conditions must be satisfied**: pulses from electrons belonging to different clusters must have a little chance of overlapping in time** and, at the same time, **the time distance between pulses generated by electrons coming from the same cluster must be small enough to prevent over-counting**.
- The fulfillment of both these requirements involves incompatible time resolutions: it appears that **the optimal counting condition can be reached only as a result of the equilibrium** between the fluctuations of those processes which forbid a **full cluster detection efficiency** and of the ones enhancing the **time separation among different ionization events**.

PId with dN/dx: first approach

- The relevant parameters for a cluster counting measurement are **the resolving time τ** and **the single electron diffusion σ_D**.
- The ideal conditions, which guarantee a real Poisson distribution of the cluster counting, are met with a resolving time **τ = 0**, in absence of diffusion, **σ_D = 0**.
- For the 90%He/10%C_4H_{10} gas mixture and a 2.5 cm drift cell, the real optimal conditions are met with **τ = 4 ns**
- It should be stressed that the obtained result is strictly related to the **detector geometry** as it depends on the impact parameter and on the dimension of the drift cell for the given gas.
- Corrections due to the track angle, impact parameter, saturation effects, attachment (for long drift) are necessary

impact parameter dependence
for 90%He/10%C_4H_{10}
12 clusters/cm

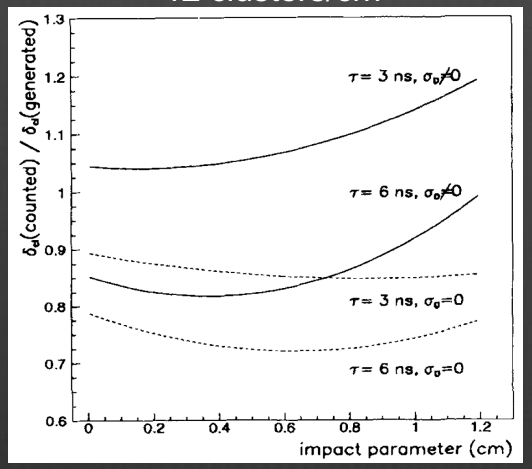

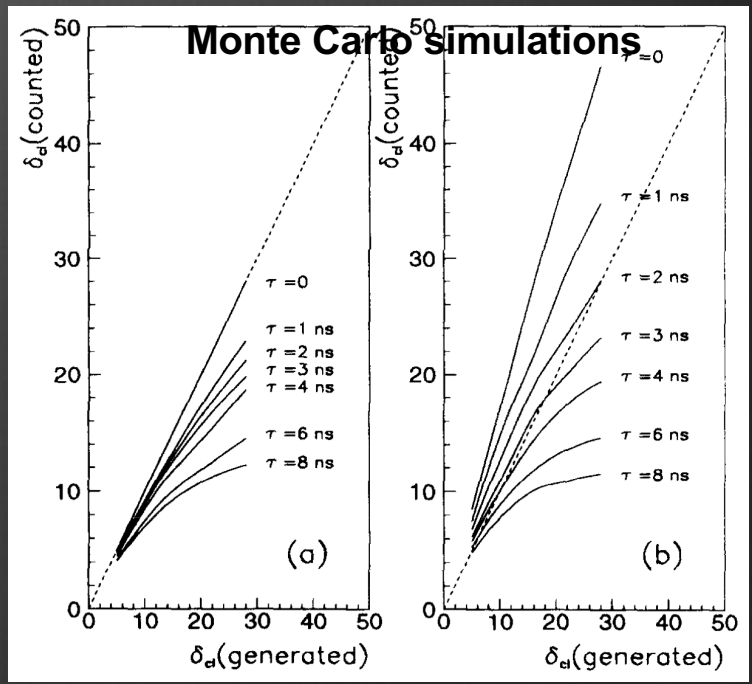

G. Cataldi, F. Grancagnolo, S. Spagnolo, *Cluster counting in helium-based gas mixtures,* **NIM A386 (1997) 458**

PId with dN/dx: second approach

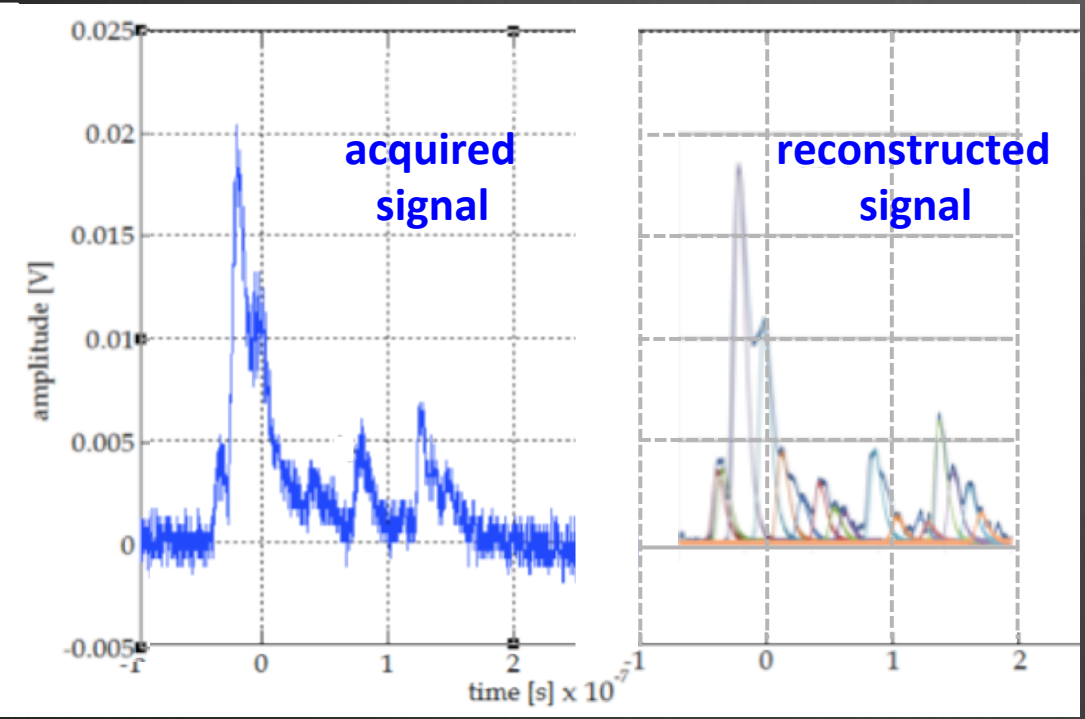

From the **ordered sequence of the electrons arrival times**, considering the average time separation between clusters and their time spread due to diffusion, one can reconstruct N_{cl} and **the most probable sequence of clusters drift times** : $\left\{t_i^{cl}\right\}\ ,\ i=1,N_{cl}$

For any given first cluster (**FC**) drift time, the **cluster timing technique** exploits the drift time distribution of all successive clusters to statistically determine, track by track, the most probable **impact parameter**, thus reducing the **bias** and improving the average **spatial resolution** with respect to that obtained from with the FC method alone.

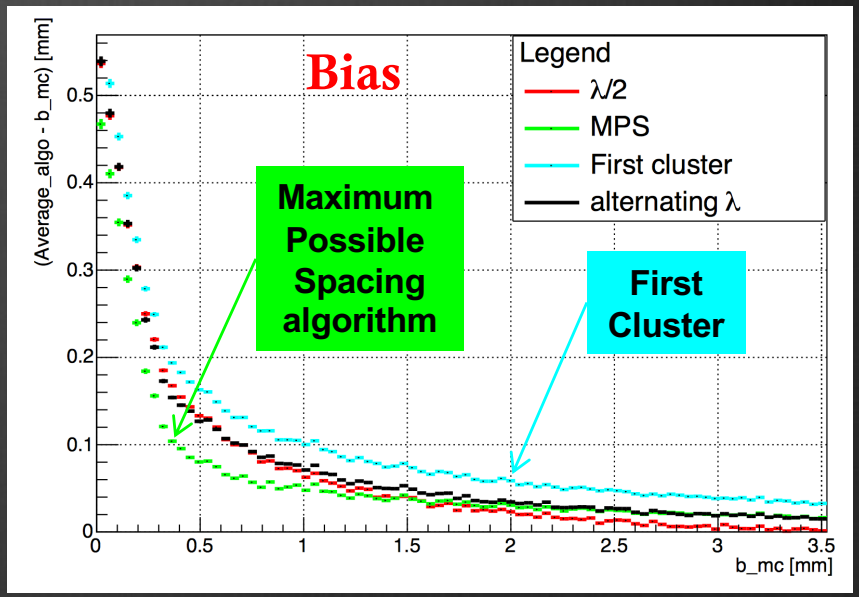

dE/dx and dN_{cl}/dx: experimental results

μ/π separation at 200 MeV/c in He/iC_4H_{10} – 95/5 100 samples 3.7 cm
gas gain 2×10^5, 1.7 GHz – gain 10 amplifier, 2GSa/s – 1.1 GHz – 8 bit digitizer

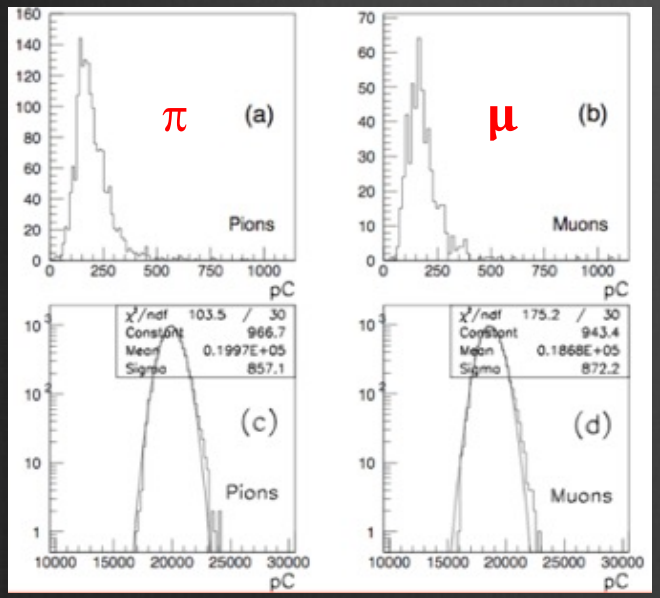

single sample
20% truncated mean

test beam data

sum over
100 samples

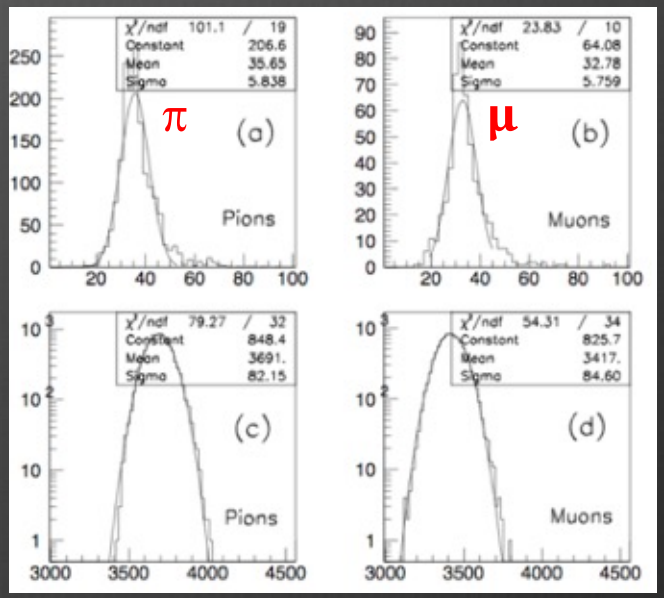

π: σ/√N$_{cl}$=0.978
μ: σ/√N$_{cl}$=1.006

π: σ/√N$_{cl}$=1.35
μ: σ/√N$_{cl}$=1.45

dE/dx separation:
2.0 σ expected
1.4 σ measured

dN/dx separation:
5.0 σ expected
3.2 σ measured

G. Cataldi, F. Grancagnolo, S. Spagnolo, *Cluster counting in helium based gas mixtures,* **NIM A386 (1997) 458**

dE/dx and dN_{cl}/dx

Expected from analytical calculation for IDEA Drift Chamber

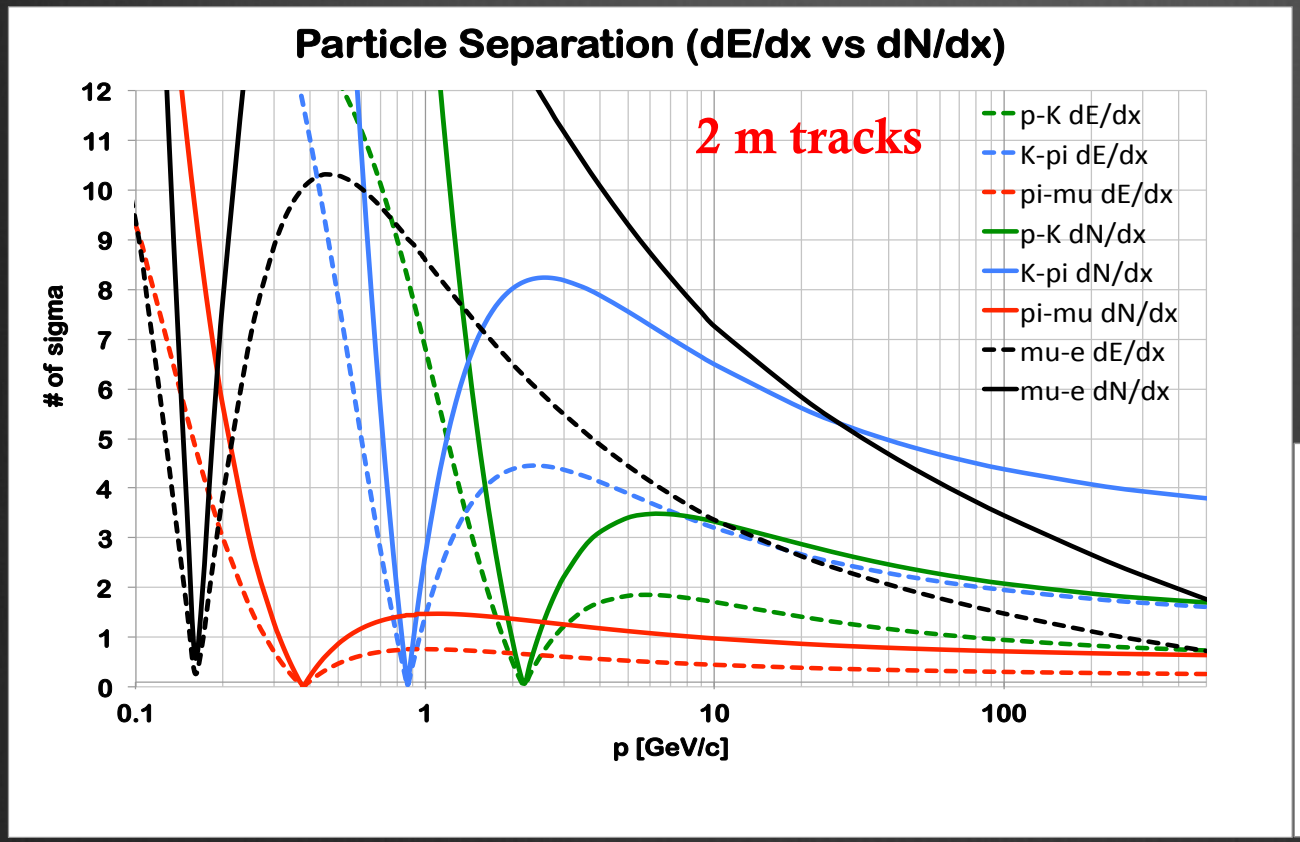

He/iC_4H_{10} 90/10
δ_{cl}(m.i.p.) = 12 cm^{-1}

σ(dE/dx)/(dE/dx) = 4.3%

80% cluster counting efficiency

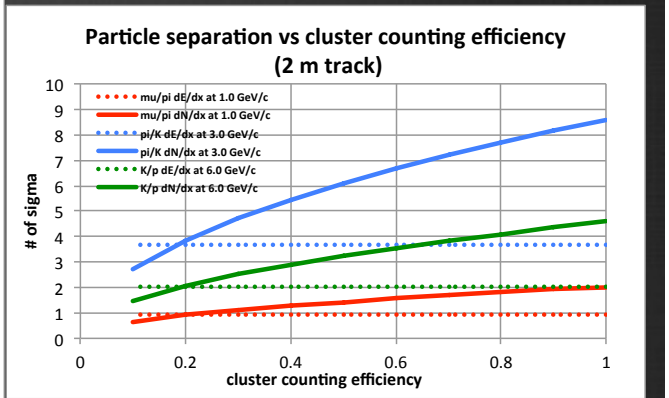

dE/dx and dN_{cl}/dx

Comments:

- **PID** comes (almost) for free in drift chambers.
- It suffers from blindness at the "crossing points", where additional technologies can be used
- **dE/dx** resolutions of around 5% are granted, provided high stability is reached on HV and gas parameters and on continuous electronics calibration.
- Alternatives to the maximum likelihood / truncated mean techniques are highly desirable (**ML**?).
- **dN_{cl}/dx** resolutions are potentially a factor 2 better than dE/dx.
- Cluster counting requires fast electronics and sophisticated counting algorithms to be fully efficient. However, given its digital nature, it is less dependent on gain stability issues.

$$\frac{\sigma_{dE/dx}}{(dE/dx)} = 0.41 \cdot N^{-0.46} \cdot \left(x_{track}[cm] \cdot P[atm]\right)^{-0.32} = 4.4\%$$

$$\frac{\sigma_{dN_{cl}/dx}}{(dN_{cl}/dx)} = \left(\delta_{cl} \cdot L_{track}\right)^{-1/2} = N_{cl}^{-1/2} = 2.2\%$$

Remarks:

- these techniques require no added complexity (and material!) to the whole detector!
- this is particularly relevant for an outer high precision EM calorimeter at a few %/sqrt(E)
- no compromise on performance and hermeticity of the detector

Conclusions

- we have presented the alternatives for tracking detectors at future e^+e^- colliders (FCC-ee, CEPC, SCTF, STCF);
- we have presented the evolution of the drift chamber concept at e^+e^- colliders over the past 40 years and given indications about the optimal configuration;
- we have summarized the **momentum resolution** obtainable with drift chambers;
- we have summarized the **particle identification** capabilities with **dE/dx** and the potentialities with cluster counting, **dN/dx;**
- we have **not** discussed about the **front-end electronics** evolution and the different techniques of **data acquisition** and **processing** of the wire signals.

- Applying, as an exercise, the above developed concepts, we ca summarize the performance of a drift chamber at FCC-ee/CEPC (**IDEA**) and at SCTF (**TraPId**):

IDEA DC and TraPId p_t resolution

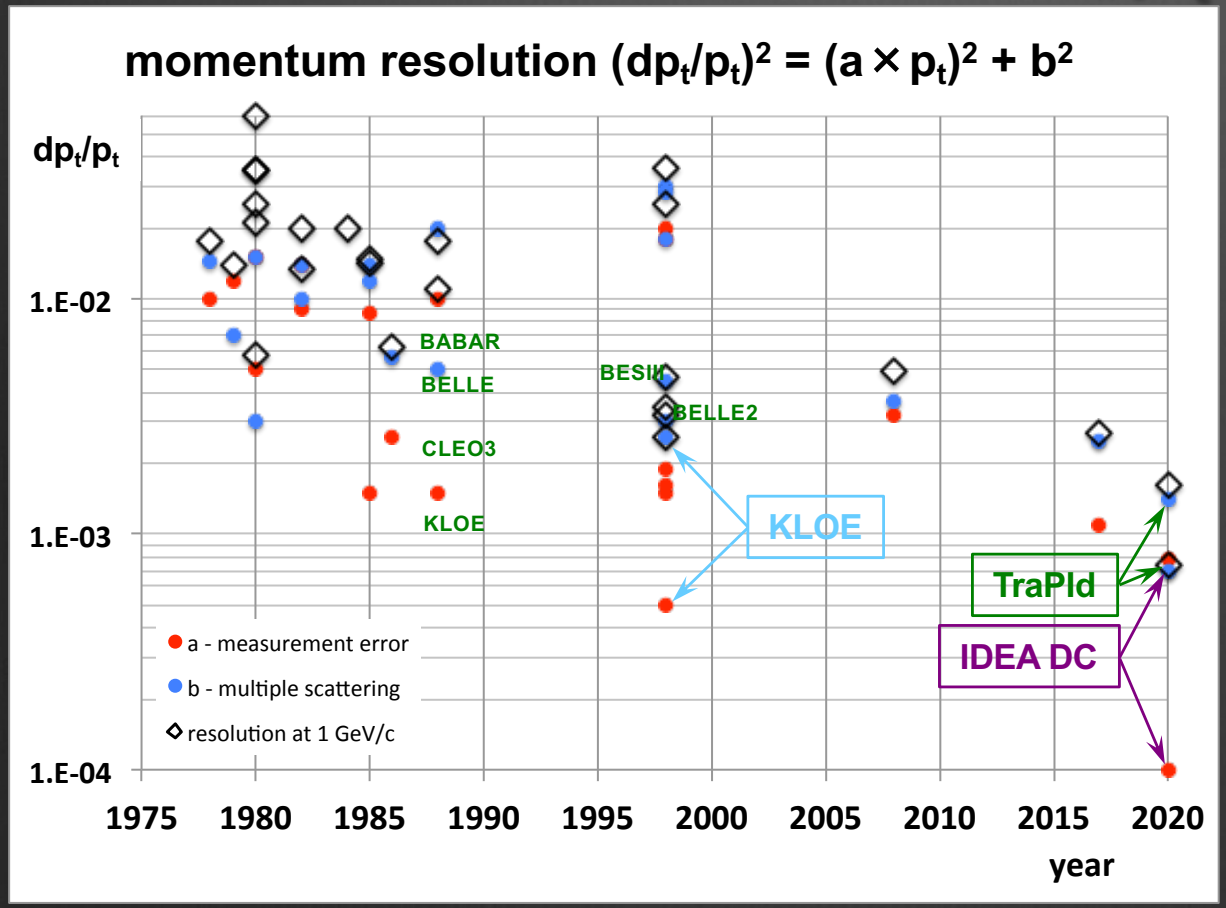

IDEA DC
proposed for the IDEA detector
at FCC-ee and CEPC

TraPId
TRAcking and Particle Identification Drift Chamber for SCTF at BINP

IDEA DC and TraPId dE/dx resolution

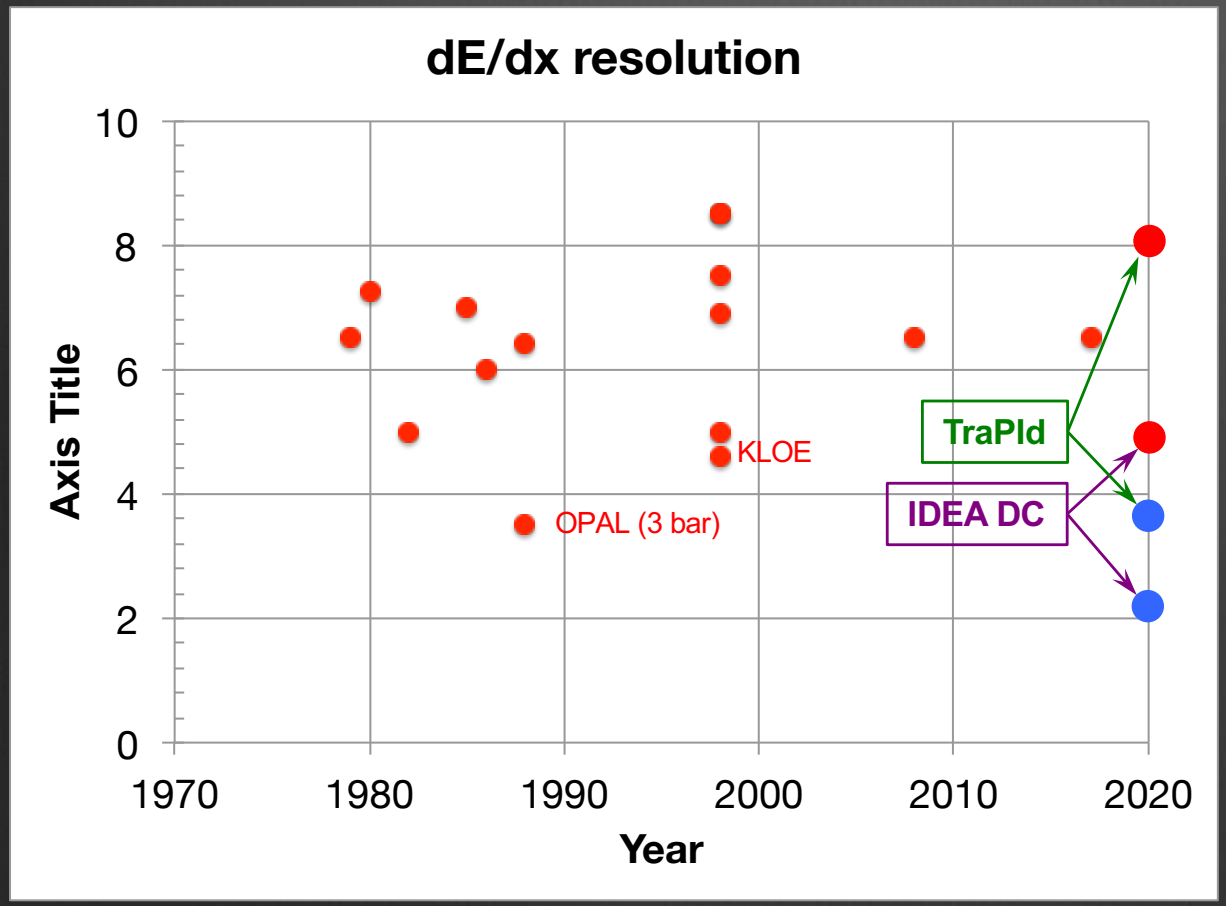

- dE/dx
- dN/dx

IDEA and TraPId end-plate X_0

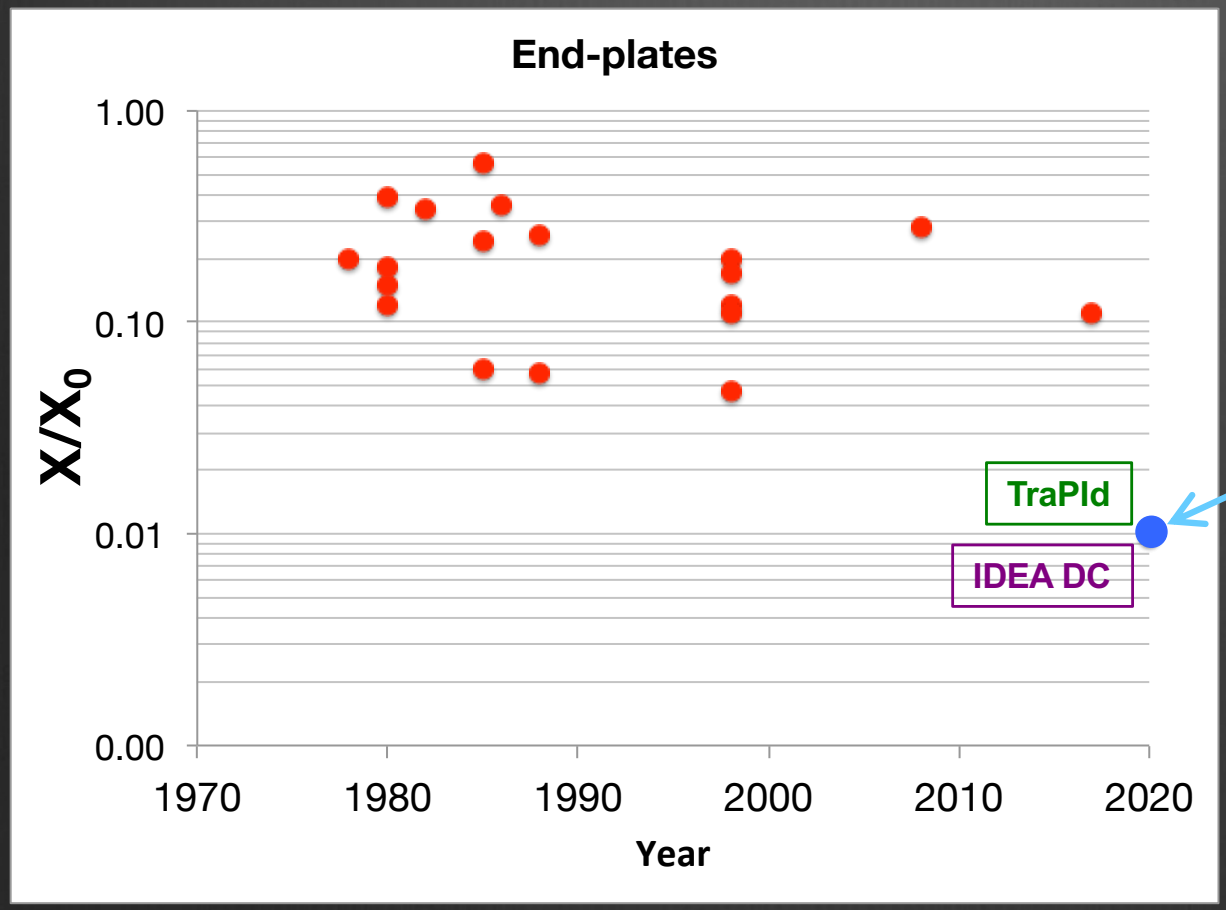

It includes the studies on

New Concepts for Light Mechanical Structures of Cylindrical Drift Chambers